2011

Direction finding in the presence of a more realistic environment model

Irfan Ahmed
Michigan Technological University

DIRECTION FINDING IN THE PRESENCE OF A MORE REALISTIC ENVIRONMENT MODEL

By

Irfan Ahmed

A DISSERTATION

Submitted in partial fulfillment of the requirements for the degree of

DOCTOR OF PHILOSOPHY

(Electrical Engineering)

MICHIGAN TECHNOLOGICAL UNIVERSITY

2011

This dissertation, "Direction Finding in the Presence of a More Realistic Environment Model," is hereby approved in partial fulfillment of the requirements for the Degree of DOCTOR OF PHILOSOPHY IN ELECTRICAL ENGINEERING .

Department of Electrical and Computer Engineering

Signatures:

Dissertation Advisor _____
Dr. Warren F. Perger

Committee Member _____
Dr. Daniel R. Fuhrmann

Committee Member _____
Dr. Jeffrey B. Burl

Committee Member _____
Dr. A. Nasser Alaraje

Department Chair _____
Dr. Daniel R. Fuhrmann

Date _____

Dedication

To My Late Parents *Abdul Shakoor* and *Safoora Khatoon*!

To My Wife *Ambreen*, Son *Humza* and Daughter *Ayesha*!

To All *Friends* and *Teachers*!

Contents

List of Figures

List of Tables

Acknowledgments

In claiming authorship to this dissertation, I am in debt of all those people who have made this possible and because of whom my graduate experience has been memorable.

My heartiest gratitude is to my advisor, Dr. Warren Perger. Whether it was luck or coincidence, I am privileged to have had an advisor who gave me the free will to investigate on my own initiative, while always ready to help in case of a fallen or missed step. It was an opportunity for me to experience the essence of the American way of research. The tolerance shown and support rendered by him enabled me to maneuver through many critical situations and finish this dissertation. His enforcement of strict validation of each result bolstered my confidence in my work. Dr. Perger has become a role model for me to follow when I will deal with my future students.

Dr. Daniel Fuhrman, despite his administrative responsibilities as department chair, has always opened his office door to me, even if it was a walk-in. I am deeply grateful to him for the extensive discussions that enabled me to cut through the technicalities of my work.

Dr. Jeffrey Burl is one of the best teachers that I have had in my life. His continuous involvement and encouragement is remarkable. He introduced me the subject of detection and estimation. The title of the dissertation underscores the significance of his expertise involved in this work.

Dr. A. Nasser Alaraje's valuable comments and guidance helped me in improving the quality of this dissertation. Dr. Brian Fick politely unfolded to me the applications of mathematics in real world situations. The mathematics involved in this work is truly a demonstration of his teachings for which I am very thankful.

I would thank the faculty members with whom I have interacted during the course of my graduate studies. Particularly, I would like to acknowledge Dr. Zhi Tian, Dr. Seyed Zekavat, Dr. Duane Bucheger, Dr. Debra Charlesworth, and Dr. Jacqueline Huntoon.

I am also grateful to the staff at Michigan Tech for their various forms of support during my graduate study, particularly, Dr. Thy Yang, Scott Ackerman, Gina Dunstan, Michele Kamppinen, Lisa Rouleau, Mark Kilpela, and Leah Jenkins. Most importantly, none of this would have been possible without the love and patience of my family. My immediate family has been a constant source of affection, care, motivation and strength all these years.

Finally, I am grateful for the major financial support from NED University, Karachi, Pakistan and the rest of the support from the Graduate School at Michigan Tech that funded parts of the research presented in this dissertation.

Abstract

Direction-of-arrival (DOA) estimation is susceptible to errors introduced by the presence of real-ground and resonant size scatterers in the vicinity of the antenna array. To compensate for these errors pre-calibration and auto-calibration techniques are presented.

The effects of real-ground constituent parameters on the mutual coupling (MC) of wire type antenna arrays for DOA estimation are investigated. This is accomplished by pre-calibration of the antenna array over the real-ground using the finite element method (FEM). The mutual impedance matrix is pre-estimated and used to remove the perturbations in the received terminal voltage. The unperturbed terminal voltage is incorporated in MUSIC algorithm to estimate DOAs. First, MC of quarter wave monopole antenna arrays is investigated. This work augments an existing MC compensation technique for ground-based antennas and proposes reduction in MC for antennas over finite ground as compared to the perfect ground. A factor of 4 decrease in both the real and imaginary parts of the MC is observed when considering a poor ground versus a perfectly conducting one for quarter wave monopoles in the receiving mode. A simulated result to show the compensation of errors direction of arrival (DOA) estimation with actual realization of the environment is also presented. Secondly, investigations for the effects on received MC of $\lambda/2$ dipole arrays placed near real-earth are carried out. As a rule of thumb, estimation of mutual coupling can be divided in two regions of antenna height that

is very near ground $0 < h < \lambda$ and fairly freespace region $h \geq \lambda$. The receiving antenna MC remains fairly unaffected from ground conductivity when the antenna height $h \geq \lambda$. Both vertical and horizontal polarization cases showed the same trend. The existing method of MC compensation by Hui(2004) is tested for the effects of nearness of good-ground to the array for azimuth DOA estimation. This investigation shows that the existing method of removing MC works well even for near ground. This result should not be confused with monopole arrays, which essentially need a perfect ground for their optimum operation.

The effects of near-zone resonant size scatterers on DOA estimation are investigated. The presence of scatterers in the near-zone of the array give cause distortion in the received signal and give rise to spurious peak in the DOA estimation spectrum. An auto-calibration algorithm for direction finding in the presence of arbitrary shaped 3D scatterers of resonating size is presented. This algorithm removes the effects of MC and 3D scatterers on direction of arrival estimation. The scatterers and wire type antenna array are excited by incident plane waves of arbitrary direction. The 3D scatterer shape is approximated as a sphere and thus spherical harmonics are assumed to be originated in response to plane wave excitation. The algorithm requires the location of the scatterers with reference to the antenna elements. However, knowledge of the exact shape of scatterers is not required. Moreover, scatterers may be located in the near or far fields. The work is supported by numerical examples for different scenarios of multiple incident waves and scatterers.

Chapter 1

Direction of Arrival Estimation in a Real Environment

1.1 Introduction

The need of localization of position arises in many civil and military applications including cellular communication, MANET, radar, radio astronomy, sonar, navigation, tracking of various objects, and other emergency assistance devices. Outdoor positioning, using global positioning systems (GPS) or techniques that measure the position of the user in a cellular network, have been well established. With the introduction of GPS, mobile wireless nodes can be equipped with the knowledge of their location. But GPS does not perform

indoors and in downtown areas due to multi-path effects. Examples of such scenarios include warehouse management, rescue services, law enforcement, and special military applications.

Hand-held devices can provide users with information on the location of interest near the user, such as fast food, amusement places, or automated teller machines. However, in emergency situations, the status and precise location of patients, care-givers, and essential equipment is required. Eventually, when the first responders come, say after a building catches fire, they receive very limited information about the structure or the location of the fire on-site. When another group of fire-fighters joins the first team, there is no way to effectively track the personnel and bring into line the entire operation. Due to the lack of location information, many trapped fire-fighters have lost their lives in the past. Similarly many lives can be saved from friendly fire by knowing the exact position of one's own troops. Thus, we need a way to measure position in an environment where satellite line-of-sight (LOS) is not available or useful [1].

Direction-of-arrival (DOA) estimation is one of the methods that are used to find the location of interest. Antenna arrays are at the forefront of any wireless device capable of DOA estimation. Environment or surroundings of the array impacts the performance of DOA estimation. The presence of arbitrary ground or near-zone scatterers are situations that cannot be ignored without compromising the performance. Traditionally DOA estimation techniques available in the literature implicitly or explicitly assume a free-space

environment for the array. Very few authors have investigated the effects of arbitrary ground or near-zone scatterers on DOA estimation. Consequently, very few techniques for such situations which are also constrained can be found in the literature. This is still an open problem and is the focus of this dissertation.

The bearing of an object with reference to the observer can be calculated by the DOA of the impinging electromagnetic waves from the object. The DOA is usually defined in spherical coordinates, elevation angle θ and azimuth angle ϕ as shown in Fig.1.1. In general, the DOA estimator is composed of directional antennas, RF front end components, and the signal processor as shown in Fig.1.2.

When a reflector antenna is used, the DOA estimator is also called the observer. In this case, the antenna should be rotated toward the direction of the source in order to

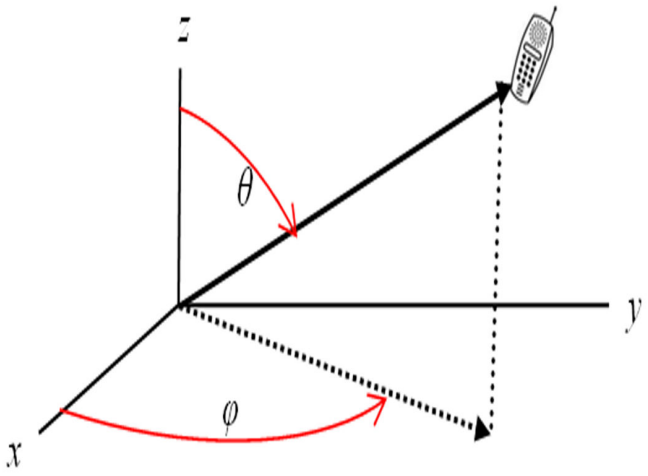

Figure 1.1: Direction of arrival of signals from a wireless device

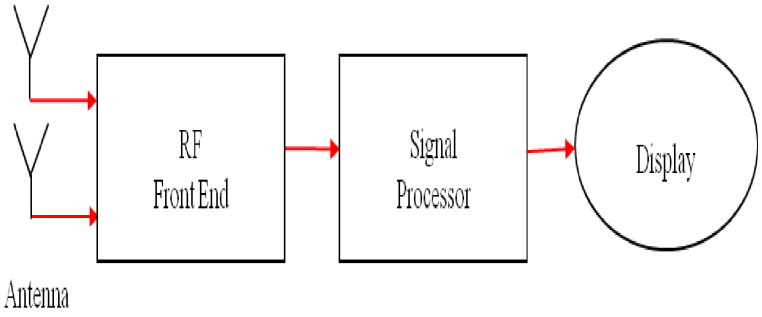

Figure 1.2: Direction of arrival estimation system

estimate the DOA. Note that an object in space can assume any azimuth or elevation angle. Traditionally, radar reflector antennas are mechanically rotated to track a moving target such as an airplane as shown in Fig.1.3. The angles at which the radar receives the strongest signal is regarded as the DOA. Some of the typically used directional antennas like Horn, Yagi, and Log periodic are shown in Fig.1.4.

The drawback of using directional antennas is the need of mechanical spinning. This

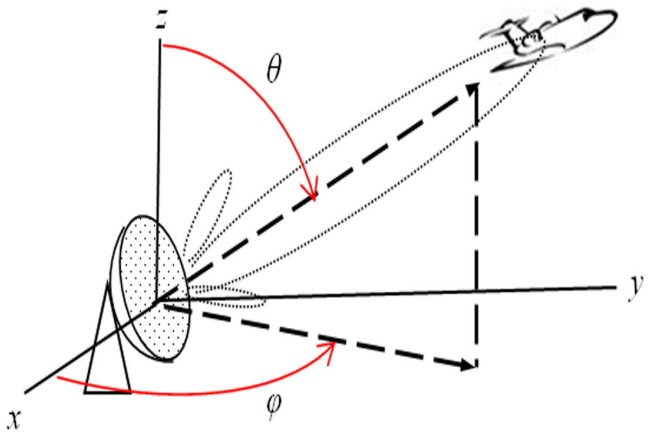

Figure 1.3: Direction of arrival of signals from a wireless device

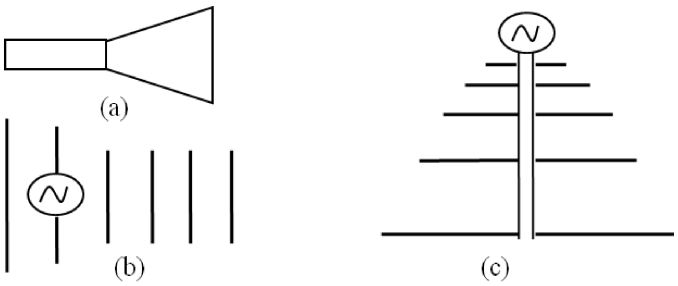

Figure 1.4: Direction antennas:(a)Horn, (b)Yagi, (c)Log Periodic

increases the power consumption, weight, size, installation and maintenance cost. The limitations in mobile platforms such as size, battery life, and weight, pose a challenge for antenna designers. One possible solution to overcome this problem is the use of antenna arrays. Antenna arrays are composed of antenna elements arranged in a geometric fashion. The main beam of an array can be rotated electronically without moving the array mechanically. Phased array antennas are examples of antenna arrays. Numerous DOA estimation algorithms have been proposed that utilize antenna arrays [2], [3].

Antennas are vital components of any wireless communication system. They are the transducers that convert transmitted electrical signals (in a wired system) to waves that propagate through space. Conversely, antennas convert the propagated signals back into electrical signals that can be detected and processed by a receiver. In other words, the receiving antenna is responsible for a reciprocal process, i.e., turning an electromagnetic wave into a signal or voltage at its terminals that can subsequently be processed by the receiver [4], [5]. Antennas can be divided into different categories, such as wire antennas, aperture antennas, printed antennas and so forth, some of them are shown in Fig.1.5.

In DOA applications, directivity is a critical antenna parameter. The directivity can be increased by increasing the electrical size of the antenna or aperture. Since it is difficult to control currents or fields of a wide aperture, discrete arrangements are often used, leading to the concept of antenna arrays shown in Fig.1.6. This formation increases the size of the antenna without actually increasing the size of the element. The array is an assembly of radiating elements in a geometrical and electrical configuration.

The individual elements of an array can be any type of antenna (wire, single reflector,

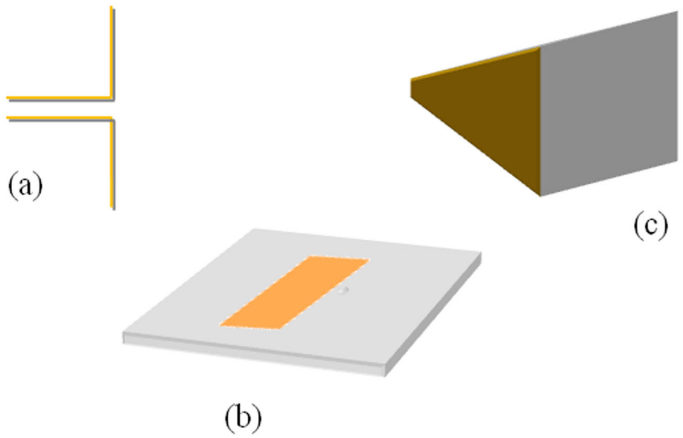

Figure 1.5: (a) Dipole (b) Printed (c) Horn, antennas

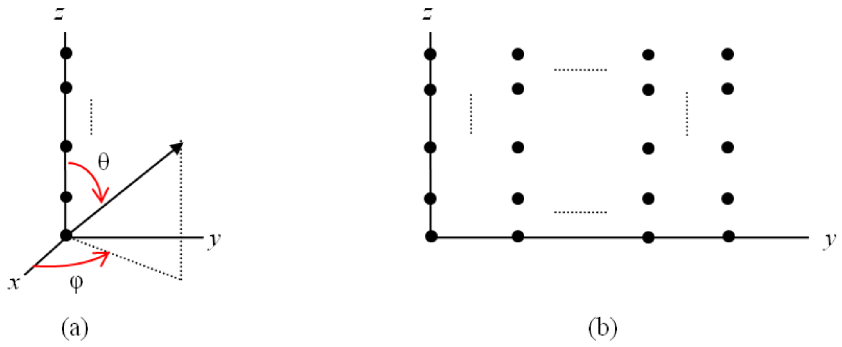

Figure 1.6: (a) Linear array, (b) Planar array, with arbitrary spacing

planar, etc.). Generally these elements are kept identical to make synthesis simpler. Placing the elements of an antenna array in a particular fashion and suitably adjusting the amplitude and phase of the individual antenna elements facilitates for the synthesis of arbitrary aperture sources. Arrays increase degree of freedom in DOA estimation by providing the ability to electronically steer the beam, combine antenna patterns, generate multiple beams, and the ability to separate multiple sources. The cost and complexity of the array and associated electronics counterbalance these advantages.

1.2 Problem Formulation

The main purpose of an antenna is to convert an electromagnetic wave into an induced voltage or current that is measured. If the antenna consists of several elements, a number of voltages or currents are measured. The physical principle that governs DOA estimation is that an incident wave reaches each antenna element at different time instants. A typical scenario is shown in Fig.1.7 where a wave is incident on an array of M elements from a source in space in the (θ, φ) direction. Suppose for the sake of simplicity that our M-element array shown in Figure (1.7) is a uniform linear array (ULA) with spacing d and we are only interested in the azimuth φ of a single narrowband source emitting signal $s(t)e^{j\omega_c t}$, where $s(t)$ is the baseband signal, $\omega_c = 2\pi f_c$ and f_c is the carrier frequency.

The received passband signals at ULA are the delayed version of the transmitted signal and

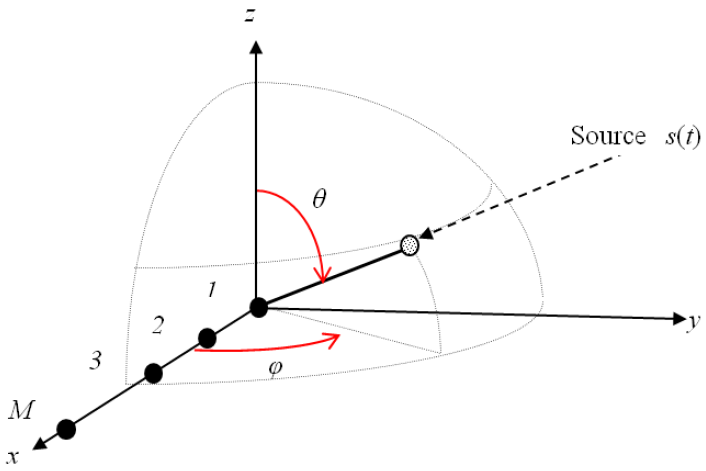

Figure 1.7: Geometry showing source *s(t)* and antenna array of M elements

corresponds to:

$$x_{pb}(t) = \begin{bmatrix} s(t-\tau_o)e^{j\omega_c(t-\tau_o)} \\ s(t-\tau_1)e^{j\omega_c(t-\tau_1)} \\ \vdots \\ s(t-\tau_{M-1})e^{j\omega_c(t-\tau_{M-1})} \end{bmatrix} \tag{1.1}$$

where τ_m is the propagation time delay for signal to reach element m. This delay is dependent on relative direction of the source from the array and given as:

$$\tau_m = \frac{md}{c}\cos\varphi \tag{1.2}$$

where $m = [0,1,\ldots,M-1]$, c is the speed of light in a vacuum and d is the spacing between the elements. The baseband signal vector after down-converting to remove the

carrier received at the array is:

$$x(t) = \begin{bmatrix} s(t-\tau_o) \\ s(t-\tau_1)e^{\frac{-j2\pi d\cos\varphi}{\lambda}} \\ \vdots \\ s(t-\tau_{M-1})e^{\frac{-j(M-1)2\pi d\cos\varphi}{\lambda}} \end{bmatrix}. \tag{1.3}$$

The received base band signal introduced in (1.3) is sampled with the sampling period of T seconds and is:

$$x(kT) = \begin{bmatrix} s(kT-\tau_o) \\ s(kT-\tau_1)e^{\frac{-j2\pi d\cos\varphi}{\lambda}} \\ \vdots \\ s(kT-\tau_{M-1})e^{\frac{-j(M-1)2\pi d\cos\varphi}{\lambda}} \end{bmatrix} \tag{1.4}$$

where, k is the discrete time index. Conventionally an array processing problem can be classified on the basis of bandwidth-delay product as following [6]:

$$\begin{cases} B\tau_m \ll 1, & \text{Narrowband;} \\ B\tau_m \gg 1, & \text{Wideband} \end{cases} \tag{1.5}$$

where, B is the bandwidth of the incident signal. In a narrowband system the signal received by any sensor is nothing but the delayed version of the signal received by all other sensors.

Therefore, in this case the time delay can well represented by phase shift. Thus, the sampled baseband signal in (1.4) corresponds to:

$$x(kT) = \begin{bmatrix} s(kT) \\ s(kT)e^{\frac{-j2\pi d\cos\varphi}{\lambda}} \\ \vdots \\ s(kT)e^{\frac{-j(M-1)2\pi d\cos\varphi}{\lambda}} \end{bmatrix}. \tag{1.6}$$

Now, we extend our problem to L available signal sources. In this case, the k^{th} sample of the l^{th} signal is denoted as $s_l[k]$ for $l = 0, 1, , L-1$. The matrix form of the signal model at the array is given as:

$$\underbrace{\begin{bmatrix} x_o[k] \\ x_1[k] \\ \vdots \\ x_{M-1}[k] \end{bmatrix}}_{\mathbf{x}} = \underbrace{\begin{bmatrix} a_o(\varphi_o) & a_o(\varphi_1) & \dots & a_o(\varphi_{L-1}) \\ a_1(\varphi_o) & a_1(\varphi_1) & \dots & a_1(\varphi_{L-1}) \\ \vdots & \vdots & \ddots & \vdots \\ a_{M-1}(\varphi_o) & a_{M-1}(\varphi_1) & \dots & a_{M-1}(\varphi_{L-1}) \end{bmatrix}}_{\mathbf{A}} \underbrace{\begin{bmatrix} s_o[k] \\ s_1[k] \\ \vdots \\ s_{L-1}[k] \end{bmatrix}}_{\mathbf{s}} + \underbrace{\begin{bmatrix} z_o[k] \\ z_1[k] \\ \vdots \\ z_{M-1}[k] \end{bmatrix}}_{\mathbf{z}} \tag{1.7}$$

where $\mathbf{x}$ is the $M \times 1$ vector of received signals at each antenna element, $\mathbf{s}$ is the $L \times 1$ vector of incident signals, $\mathbf{z}$ is the $M \times 1$ vector of white Gaussian noise with mean zero and variance σ^2 appearing at the antenna terminals and $\mathbf{A}$ is the set of all direction vectors $\mathbf{a}(\varphi)$

matrix known as the array manifold [3] with order $M \times L$. Columns of the array manifold are called steering vectors, each corresponds to a DOA φ_l and is denoted as $\mathbf{a}(\varphi_l)$. The frequency domain signal model for DOA estimation in compact form is given as:

$$\mathbf{x} = \mathbf{A}\mathbf{s} + \mathbf{z}. \tag{1.8}$$

The model given in (1.8) considers each antenna element as if it were in free-space. Later in this chapter, effects of the surrounding environment and mutual coupling between elements on DOA estimation will be discussed. Assuming $\mathbf{s}$ and $\mathbf{z}$ are uncorrelated, the spatial covariance matrix of (1.8) is given as:

$$\mathbf{R} = \mathbf{A}E[\mathbf{s}\mathbf{s}^H]\mathbf{A}^H + \sigma^2\mathbf{I} \tag{1.9}$$

where $\sigma^2\mathbf{I}$ is the correlation matrix of the measurement noise $\mathbf{z}$, $\mathbf{I}$ is an $M \times M$ identity matrix with $M > L$. The matrix $\mathbf{R}$ is Hermitian with real eigenvalues. The eigendecomposition of $\mathbf{R}$ can be given by [7]:

$$\mathbf{R} = \mathbf{U}\mathbf{W}\mathbf{U}^H = \begin{bmatrix} \mathbf{U}_s & \mathbf{U}_z \end{bmatrix} \begin{bmatrix} \mathbf{W}_s & 0 \\ 0 & \sigma^2\mathbf{I} \end{bmatrix} \begin{bmatrix} \mathbf{U}_s & \mathbf{U}_z \end{bmatrix}^H. \tag{1.10}$$

Given $M > L$, matrix $\mathbf{W}$ is a diagonal matrix of eigenvalues placed in non-ascending order. The matrix $\mathbf{W}_s$ contains L eigenvalues, while $M-L$ smallest eigenvalues are in the matrix $\sigma^2\mathbf{I}$, where $\mathbf{I}$ is of order $M-L \times M-L$. The matrix $\mathbf{U}$ contains the eigenvectors of $\mathbf{R}$. This matrix is portioned into $\mathbf{U}_s$ that contains L eigenvectors and $\mathbf{U}_z$ that contains $M-L$ eigenvectors. The spaces spanned by $\mathbf{U}_s$ and $\mathbf{U}_z$ are known as the signal and noise subspace, respectively.

1.3 DOA Estimation Methods

There are numerous methods available in the literature to estimate DOA such as beam-forming [8], MUSIC [9], ESPRIT [10] and maximum-likelihood direction estimation [11]. A detailed overview is available in [12]. In this dissertation we used a classical beam-forming technique "delay-and-sum " and a super-resolution technique "MUSIC", which are briefly described here by considering the signal model of (1.8).

1.3.1 Delay-and-Sum

This method is based on a simple beamforming concept also known as spatial filtering. A beamformer acts like a filter that enhances the desired signal power and reduces the interference signal power. The output power of the beamformer is a function of DOA and

is given as [8]:

$$P(\varphi) = \mathbf{a}(\varphi)\mathbf{R}\mathbf{a}(\varphi)^H \tag{1.11}$$

where $\mathbf{R}$ is introduced in (1.9). The $P(\varphi)$ pattern will have peaks in the direction of the incident source.

1.3.2 MUSIC

MUSIC (MUltiple-SIgnal-Classification) is a relatively simple and efficient eigenstructure DOA estimation method [14]. This method can be applied to any arbitrary array geometry. To find DOAs, this method searches through the set of all possible steering vectors and finds those that are orthogonal to the noise subspace. Using signal model for DOA estimation (1.8), and the eigendecomposition of spatial covariance matrix (1.10), the MUSIC spectrum is given as:

$$P_{MUSIC}(\varphi) = \frac{1}{\mathbf{a}(\varphi)^H \mathbf{U}_z \mathbf{U}_z^H \mathbf{a}(\varphi)}. \tag{1.12}$$

This is an all-pole spectrum and yields a very high value at the DOA angles. MUSIC is also known as a super-resolution method as it breaks the barrier set by the Rayleigh resolution

limit. MUSIC is perhaps the most studied method in its class and has many variants such as Root-MUSIC [13], [14].

1.4 Errors in DOA Estimation

Generally for wireless, and particularly for the mobile environments, DOA finding encounters different types of errors resulting in uncertainty of estimation. These may be classified in terms of the following [7]:

- *Signal model errors*: Signals may be wideband instead of narrowband, and emitters may be in the nearfield causing the plane wave incidence assumption to be invalid.
- *Array model errors*: Variations may exist in the gain and phase responses of the sensors, and mutual coupling may occur between antenna elements.
- *Propagation model errors:* The real environment may not be homogeneous (e.g., near-zone scatterers, and the propagation environment may vary (e.g., due to weather); thus, the scattering environment may be varying with time and space.

In this dissertation we are focusing on a more realistic environment which surrounds our antenna. Thus, the errors in DOA estimation arising from the immediate surrounding of the array is of our prime concern. Therefore, we will limit ourselves to discussing the two major sources of error: near-ground mutual coupling creating array modeling errors and

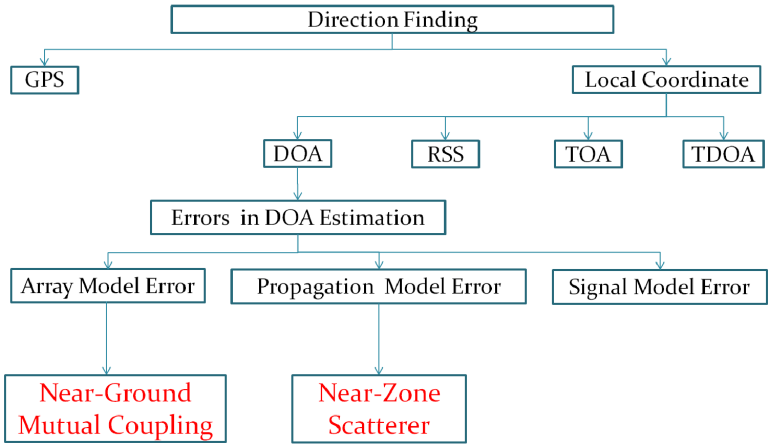

Figure 1.8: Scope of the dissertation

the presence of near-zone scatterers creating propagation model errors. Fig.1.8 describes the scope of the work carried out in this dissertation.

1.4.1 Impact of Array Mutual Coupling

The signal model for DOA estimation (1.8) assumes ideal antenna arrays, i.e., there is no interaction across antenna elements. However, in a real array, fields from each antenna element interact with other antenna elements causing mutual sharing of energy that is called mutual coupling [15]. The strength of the mutual coupling is mostly determined by the element type (its radiation characteristics), the distance between the elements, and how the elements are oriented relative to one another [4]. An array can be flexibly operated in transmitting mode or receiving mode. Consequently, mutual coupling for one mode has a distinct definition and perspective from the other[16].

Consider a pair of antenna elements as a part of an array operating in the transmitting mode as shown in Fig.1.9. The exciter attached to the input port of antenna #n establishes an outward traveling wave from the source to the antenna element marked as (0). The resulting radiation divides in two parts: radiation towards infinite space (1), and radiation directed to antenna #m (2). The later is known as the coupled energy and causes current flow in antenna #m. The field due to this current flow again divides in two parts: reradiation towards infinite free space(3), and traveling wave towards the source attached to antenna #m (4). However, the reradiated wave (3) divides itself in a similar way as done by (0), and so forth. Thus the resultant farfield pattern of any of the single element in the array has the energy contribution not only from its own exciter, but also from the excitations due to the mutual coupling among the elements.

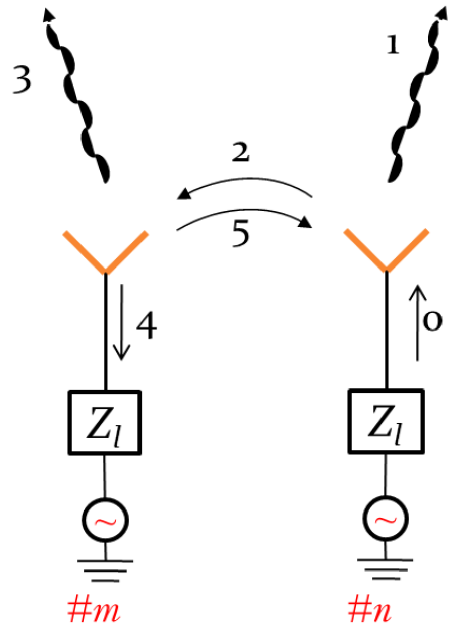

Figure 1.9: Transmitting mode mutual coupling; After [16]

Now consider a pair of elements from a similar array operating in the receiving mode with passive loads attached to its terminals as shown in Fig.1.10. Suppose a plane wave is incident upon the array from such direction that it reaches antenna #m first. This results in an induced traveling wave from antenna towards the passive load (1), and scattering of part of the incident field; back into the space (2), and towards the neighboring antenna elements (3). The later adds vectorially to the principal field incident upon antenna #n. Thus, the total received energy at a particular antenna terminal is composed of direct incident field, and coupled fields from other antenna elements in the array. The DOA estimation generally encounters receiving mode mutual coupling [17].

In order to incorporate the effects of mutual coupling in DOA estimation the signal model in (1.8) is modified as [18]:

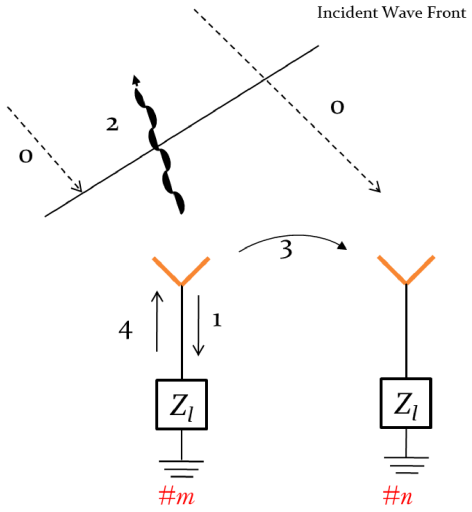

Figure 1.10: Receiving mode mutual coupling; After [16]

$$\mathbf{y} = \mathbf{CAs} + \mathbf{z} \tag{1.13}$$

where $\mathbf{y}$ is the received signal in the presence of mutual coupling. $\mathbf{C}$ is the matrix whose complex coefficients perturbs the received signals. Assuming that the noise process and phenomenon of mutual coupling are independent of each other, the covariance matrix (1.9) becomes:

$$\mathbf{R} = \mathbf{CA}E[\mathbf{ss}^H]\mathbf{C}^H\mathbf{A}^H + \sigma^2\mathbf{I}. \tag{1.14}$$

Now, the signal eigenvectors do not span the same subspace as the array manifold, but the one spanned by matrix $\mathbf{CA}$. Then, it is necessary to estimate the coupling matrix and introduce it into the DOA algorithm to avoid errors. If the mutual coupling matrix is unknown, or only approximately known, an error is introduced in the signal model. Generally, there is no defined structure for the $\mathbf{C}$ matrix. It is in the literature that the mutual coupling coefficients are inversely proportional to the distance between elements [18]. Therefore, as the the distance between two elements increases the magnitude of the corresponding coefficients in $\mathbf{C}$ diminishes and approaches zero. Hence, a banded matrix furnishes a reasonable model for a ULA [18]. In a banded matrix the non-zero entries are confined to a diagonal band, comprising the main diagonal and zero or more diagonals on either side [19]. Also, the coupling between any equally spaced pair of elements is equal and is independent of the location of the pair within the array. Therefore, matrix $\mathbf{C}$ of an

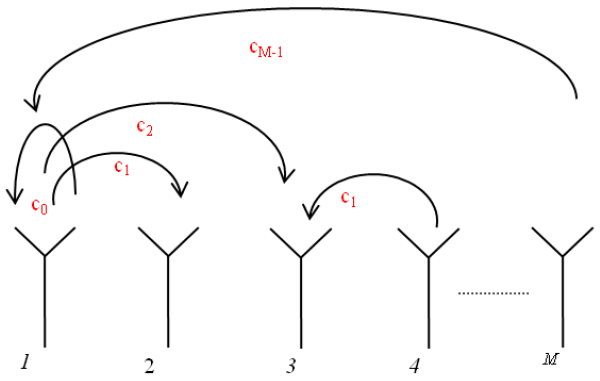

Figure 1.11: Mutual coupling coefficients for a ULA assuming a banded Teoplitz structure

ideal ULA can be best represented by a banded Toeplitz mutual coupling matrix, see Fig (1.11). The banded Toeplitz mutual coupling matrix of an M elements ULA can have a maximum of $M-1$ nonzero coefficients and given as:

$$C_{ULA} = \begin{bmatrix} c_o & c_1 & \dots & c_{M-1} \\ c_1 & c_o & \ddots & \vdots \\ \vdots & \ddots & \ddots & c_1 \\ c_{M-1} & \dots & c_1 & c_o \end{bmatrix}. \tag{1.15}$$

A number of techniques for the compensation of errors in DOA estimation due to the mutual coupling, are available in the literature and some of these will be reviewed in Section 1.5.1.

1.4.2 Impact of Near-Zone Scatterer

In the previous section, we asserted that compensation for mutual coupling is necessary to remove its effects from DOA estimation. However, the errors removed by this compensation belong to the class of the array model errors which implicitly assumes that the antenna array is in free-space. In a real deployed scenario, the presence of objects in the near field causes the antenna to interact with them and invalidates the free-space assumption [20]. Proximity of an imperfect ground and a metal chassis are examples of such objects that cause distortion of the signal and produce errors in DOA estimation [21]. It is also reported in the literature that an array calibration that does not takes into account the presence of near-zone scatterers may produce spurious peaks in spectral DOA estimation [22].

Most of the DOA estimation methods assume that sources are in the farfield and, therefore incident waves are plane waves. This assumption is generally valid with the free-space assumption. As shown in Figure 1.12, the nearfield scatterer produces spherical waves, when illuminated by farfield sources. Thus, the total received voltage $\mathbf{V}^t$ at the antenna terminals is composed of two components, one due to the incident plane wave $\mathbf{V}^{inc}$ and other one due to the spherical waves from the scatterer $\mathbf{V}^{sct}$ as:

$$\mathbf{V}^t = \mathbf{V}^{inc} + \mathbf{V}^{sct} \tag{1.16}$$

This hinders the ability of any DOA estimation method to resolve two incident plane waves with a small angular separation [23]. The plane waves from the farfield are desired signals, and spherical waves are the interfering signals.

Section 1.5.2 gives an overview of the available techniques to overcome the effects of this propagation model error on DOA estimation.

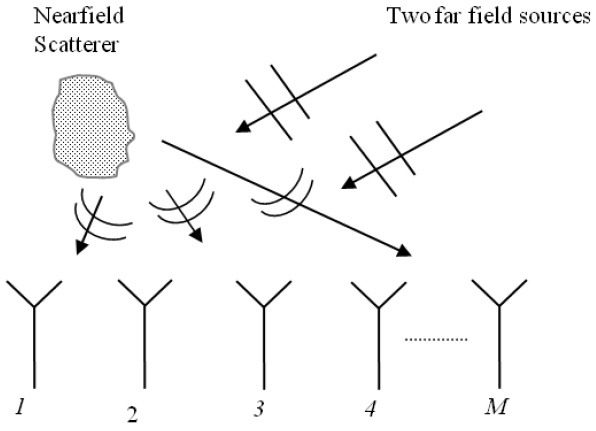

Figure 1.12: Spherical wave generation due to plane wave incidence in the presence of a nearfield scatterer; After [23]

1.5 Available State-of-the-Art Techniques

The state-of-the-art techniques to compensate for errors in DOA estimation due to mutual coupling and near-zone scatterers are in the process of evolution. For the purpose of this dissertation, approaches are broadly classified in two groups. The first one includes the techniques for compensating for mutual coupling while the second one encompasses compensating techniques for near-zone scattering effects. Each group is further subdivided into pre-calibration and auto-calibration techniques.

1.5.1 Compensation Techniques for Mutual Coupling

A number of techniques from signal processing [18], [24], [25], electromagnetics[15], [26], [27], [17] and advance optimization such as genetic algorithms [28] and simulated annealing [29] are in the literature to compensate for errors in DOA estimation due to mutual coupling. These techniques in general seek the coefficients of $\mathbf{C}$ in the signal model of (1.13). By and large, these methods assume a free-space environment around the antenna. Thus, any error in the propagation model, which generally assumes plane wave incidence due to the farfield sources, can not be removed. Most of them apply certain restrictions on the structure of $\mathbf{C}$, such as $\mathbf{C}$ is Toeplitz. Some compensatory methods work only with a certain DOA estimation technique; thus, they also carry the restrictions

of the parent. A short overview of some well-referred techniques is given in this section by grouping them in terms of Pre-calibration and Auto-calibration.

1.5.1.1 Pre-Calibration

In the pre-calibration methods the perturbation in measurement due to mutual coupling and gain/phase errors is estimated or known prior to DOA estimation. One way is to estimate the perturbation matrix $\mathbf{C}$ by numerical techniques such as method of moments (MoM). The other way is to experimentally determine the relation between the perturbed measured voltages and the ideal or theoretical voltages by using external sources at known angles. Usually this is done in an isolated environment or anechoic chamber. These methods do not impose any restriction on the structure of the coupling matrix and provide a better realization of the problem. In general, these techniques are model-specific; that is, limited to a certain type of antenna and surrounding environment. Moreover, these techniques do not address a very important source of error; namely the proximity of real-earth and its effects on mutual coupling.

The relation between the theoretical array manifold $\mathbf{A}$ and the perturbed array manifold $\mathbf{A}_c$ is given as

$$\mathbf{A}_c = \mathbf{CA} \tag{1.17}$$

where $\mathbf{A}_c$ is perturbed by the errors due to mutual coupling and sensor gain & phase errors. Therefore, the matrix $\mathbf{C}$ can be considered as the distortion matrix. In general, $\mathbf{A}_c$ depends on the direction of the incoming signal changes. In [26] the MoM is used to determine $\mathbf{A}_c$ for a few observation angles. The method assumes that the current shape on a ULA of thin wire antennas such as dipole remains unchanged for any azimuth direction(fixed elevation angle θ) in response to plane wave excitations. Therefore, matrix $\mathbf{C}$ of the array can be obtained by using the pseudo-inverse concept which corresponds to:

$$\mathbf{C} = \mathbf{A}_c\mathbf{A}(\mathbf{A}\mathbf{A}^H)^{-1} \tag{1.18}$$

Another method [27] is based on MoM but is more accurate in calibration as it does not assume independence of current shape from the direction of incidence. Instead of estimating $\mathbf{C}$, this method finds $\mathbf{A}_c$ for all azimuth incidence and stores them for online use for DOA estimation.

In experimental methods for array calibration for DOA estimation, the relation between $\mathbf{V}_{actual}$ which carries the mutual coupling effects to the $\mathbf{V}_{ideal}$ which assumes that each antenna element is in isolation from all other elements is given as:

$$\mathbf{Z}\mathbf{V}_{actual} = \mathbf{V}_{ideal} \tag{1.19}$$

where dimensionless matrix $\mathbf{Z}$ is known as impedance matrix and carries mutual coupling coefficients normalized by terminal load impedance. Thus, the M element array can be treated as an M port network from classical circuit theory.

One such method that terms $\mathbf{V}_{ideal}$ as open circuit voltage [15] . Let $Z_{ij}, (i, j = 1, 2, \ldots, M)$ be the mutual impedance between antenna elements i and j and given as [4]:

$$Z_{ij} = \frac{V_{oci}}{I_j} \tag{1.20}$$

where V_{oci} is the open circuit voltage measured at i_{th} antenna terminal in response to a feed point current flowing in the j_{th} antenna terminal. Much has been reported in the literature about the difference in transmission and receiving mode mutual impedance [16]. Therefore, this method has a shortcoming of assuming the array is in transmission mode, while in practice most of the arrays work in receiving mode for DOA estimation.

The receiving mutual impedance method was proposed to realize the receiving mode mutual impedance [17]. This method used an external plane wave source to excite the array of wire type antennas to estimate mutual impedance. It takes into account antenna terminal load and also incorporates radiation from all other elements in the mutual impedance measurement. The voltage $\mathbf{V}_{ideal}$ is considered as isolated terminal voltage as if antenna element is completely isolated from the array.

1.5.1.2 Auto-Calibration

In the auto-calibration approach, also termed self-calibration, simultaneous DOA estimation of desired sources and coefficients of matrix **C** is carried out. Thus, no additional source is required to calibrate the array. The instantaneous estimation of **C** is used in the signal model (1.13) to remove the errors due to the mutual coupling. In general, the auto-calibration methods available to date are not straightforward in guaranteeing uniqueness of the solution and this limits their practical use. An overview of self-calibration methods is available in [30] for interested readers.

In [18] an iterative algorithm is proposed to estimate simultaneously both DOA and mutual coupling parameters. It assumes a banded Toeplitz structure of **C** for uniform linear or circular arrays. It is the minimization of the following cost function J as:

$$J = \sum_{l=1}^{L} \|\hat{\mathbf{U}}_z \mathbf{C}\Gamma\mathbf{a}(\varphi_l)\|^2 \tag{1.21}$$

where $\hat{\mathbf{U}}_z$ is the estimated noise subspace $\mathbf{U}_z$ defined in (1.10), **C** is the mutual coupling matrix, Γ is the diagonal antenna gain/phase matrix and $\|.\|^2$ is the squared Euclidean norm.

This published algorithm is composed of three steps. First, it assumes that the gain / phase and mutual coupling coefficients are (approximately) known. Second, the numbers of DOA's L are found by using the standard MUSIC algorithm. Given the estimates of number

of DOAs, J is minimized over the gain /phase parameters. Given gain/ phase parameters and number of DOA's, J is minimized over the components of $\mathbf{C}$. These minimization process is iterated until J converges. However, the method is limited in application to MUSIC like algorithms because it uses eigenstructure approach to estimate DOA and related parameters. Moreover,it cannot provide a unique solution.

An online mutual coupling compensation algorithm for ULAs is proposed in [24]. This iterative algorithm simultaneously compensates for mutual coupling and estimates the direction-of-arrivals (DOAs) of signals impinging on the array. In order to exploit ULA structure, the method can not consider the effects of sensor gain-phase in the estimation of DOAs. It also assumes Toeplitz structure of $\mathbf{C}$, thereby implicitly assuming the free-space environment. No mathematical proof of solution uniqueness is provided in the description of method.

A non-iterative algorithm for finding the DOAs in the presence of mutual coupling of an M-element ULA is proposed in [25]. The algorithm is based on the GEESE method which is the abbreviation for Generalized Eigenvalues utilizing Signal Subspace Eigenvectors. The $\mathbf{C}$ is assumed to have banded symmetric Toeplitz structure. The method does not explain how it estimates the number of sources L before initializing the estimate. In addition, uniqueness of the solution requires a large number of antenna elements.

1.5.2 Compensation Techniques for Near-Zone Scattering

A limited number of authors addressed the issue of near-zone scatterers for DOA estimation. Most of the methods are model specific, that is, for a certain array and surrounding. Some that pose to be generic either consider 2D scatterers or fail to guarantee global optimum solution. To remain consistent with this dissertation, these methods are divided in terms of Pre-calibration and Auto-calibration.

1.5.2.1 Pre-Calibration

A near-field scattering problem such as the presence of a conducting plate behind the array elements is discussed and some solutions were proposed [31]. To accurately account for structure scattering, the paper considers coupling matrix as non-square. This method requires knowledge of scatterer geometry. This limits its application to fixed antennae whose surrounding remains unchanged.

A non-conventional least square optimization method is proposed to exploit the large data set of pre-calibrated steering vectors for DOA estimation with near-zone scatterers [22]. This method is limited to ULA of dipoles with a fixed geometry of the problem. Once the position or type of scatterer changes, the calibration can no longer help in sufficient reduction of DOA estimation error.

1.5.2.2 Auto-Calibration

A self-calibration technique for DOA estimation using the MUSIC algorithm where an uncoupled near-field scatterer is present is in the literature [23]. This method does not remove the effects of mutual coupling and works only for 2D scatterers. Another self-calibration algorithm that removes the effects of mutual coupling and near-zone scatterers is also in the literature [32]. This algorithm approximates a scatterer as a cylinder and, therefore assumes cylindrical harmonic expansion origination in response to a plane wave incidence [33] . The algorithm is iterative and does not guarantee the achievement of the true DOA but rather convergence. It also works only for 2D scatterers and requires a large number of antenna elements.

1.6 Overview of Dissertation

The short review of the literature in section 1.5 points to the need of further work in this direction. It is seen that techniques for compensating for errors in DOA estimation due to mutual coupling are constrained by various parameters such as specific DOA method, particular antenna type, shape of array, etc. One important aspect which is ignored either implicitly or explicitly is the presence of real-earth in the proximity of the antenna. This dissertation addresses the issue by investigating and proposing a compensation approach

in Chapters 2 and 3. Two types of antenna elements are selected for investigation, each having a peculiar relationship with the ground. The first type is a monopole antenna which is a ground-based antenna and through image theory needs a perfect ground for its operation. The effects of arbitrary earth on mutual coupling of monopole antenna array are investigated and compensatory proposals for DOA estimation are presented in Chapter 2. The second type, a dipole antenna which is presumably an omnidirectional antenna in the absence of any ground plane, is investigated for mutual coupling effects and compensatory proposals and presented in Chapter 3.

It is also evident that compensation for errors in DOA estimation due to the presence of near-field scatterers is a fairly open problem. Particularly for portable wireless devices, a model-based approach is not helpful. The self-calibration techniques are limited to the 2D scatterers despite other constraints. This work also proposes an algorithm for DOA estimation that is more realistic in approach because it considers 3D scatterers in near-zone (see chapter 4).

In order to remain consistent with the way the literature is reviewed in Section 1.5, this dissertation can be classified as pre-calibration techniques Chapters 2 and 3 for mutual coupling compensation and auto-calibration technique Chapter 4 for compensating errors due to the presence of near-zone scattering.

1.6.1 Pre-Calibration

In chapter 2, the effects of ground constituent parameters on the mutual coupling (MC) of a monopole antenna array are investigated. This work augments an existing MC compensation technique for ground-based antennas, and proposed reduction in mutual coupling for antennas over finite ground as compared to the perfect ground. The work is investigated by finite element method analysis and numerical results are presented. A factor of 4 decrease in both the real and imaginary parts of the mutual coupling is observed when considering a poor ground vs. a perfectly conducting one, for quarter-wave monopoles in receiving mode. A simulation result shows the errors in direction of arrival (DOA) estimation with actual realization of the environment is also presented.

Chapter 3 investigates the effects on received mutual coupling of $\lambda/2$ dipole arrays placed near real-earth. As a rule of thumb, estimation of mutual coupling can be divided in two regions of antenna height that is very near ground $0 < h < \lambda$ and fairly free-space region $h \geq \lambda$. The receiving antenna mutual coupling remains fairly unaffected from ground conductivity, when antenna height $h \geq \lambda$. Both vertical and horizontal polarization cases showed the same trend. Investigation of effects of nearness of good-ground to the array on DOA estimation revealed that for azimuth DOA estimation, the existing method of removing mutual coupling works well even for near ground. This result should not be confused with monopole arrays, which essentially need a perfect ground for their optimum

operation.

1.6.2 Auto-Calibration

In chapter 4, a self-calibration algorithm for direction finding in the presence of arbitrary shape 3D scatterers of resonating size is presented. This algorithm removes the effects of mutual coupling and 3D scatterers on direction-of-arrival estimation. The scatterers and wire type antenna array are excited by incident plane waves of arbitrary direction. The 3D scatterers can be of any shape but is approximated as a sphere, thus, spherical harmonics are assumed to be originated in response to the plane wave excitation. The algorithm requires the location of the scatterers with reference to antenna elements. However, knowledge of exact shape of scatterers is not required. Moreover, scatterers may be located in near or far fields.The work is supported by numerical examples for different scenarios of multiple incident waves and scatterers.

Chapter 2

Effects of Ground Constituent Parameters on Array Mutual Coupling for DOA Estimation*

2.1 Introduction

There is an emerging trend in wireless applications such as safety and security, command and control, and MIMO communication that requires antennas with direction-of-arrival (DOA) and beamforming capability. In order to implement this capability, antenna arrays

*Parts of this chapter have been published in *International Journal of Antennas and Propagation*. The paper is open access and distributed under the Creative Commons Attribution License [34].

are used. Traditionally, antenna arrays consist of closely located antenna elements that are uniformly distributed across the array. To determine DOA, several techniques have been developed [8]. These techniques frequently assume that the sensors are ideal and operate in an isolated environment. In practice, however, this is not true. The real antenna elements not only interact with each other due to mutual coupling (MC) but also with the surroundings. This results in the distortion of the signal and causes error in DOA estimation.

Several techniques have been proposed to overcome the errors due to antenna MC. These techniques are in the process of development, but can be classified in terms of auto-calibration [18], [24], [25], open circuit voltage method [15], numerical techniques [26], [27], [28], offline calibration [35] and receiving mutual impedance methods [17]. In general, these techniques do not consider the interaction of the antenna array with an imperfect ground in the near-zone [36]. Effects of ground proximity and constituent parameters on wire antennas have been presented in the literature [37], [38], [39].

This chapter considers the effects of ground on the MC of an array of monopoles and its impact on DOA estimation. Monopole antennas that take advantage of image theory are ideally placed above a perfect ground of conductivity $\sigma = \infty$ and relative permittivity $\varepsilon_r = 1$. The real ground or earth has finite conductivity and may have high permittivity. The effects of ground constituent parameters on MC and ultimately to DOA estimation are investigated. The evaluation of MC is an extension of the technique that finds MC of a

monopole array over a high conductivity ground ($\sigma \cong 10^7, \varepsilon_o, \mu_o$) [17] to a finite ground ($\sigma \leq 1, \varepsilon, \mu_o$). The newly-found MC is used to compensate error in the DOA estimation for an array over imperfect ground.

2.2 Problem Formulation

Consider a uniform linear array (ULA) of M omnidirectional elements. Suppose plane waves from J narrowband farfield sources are incident on this array and $(M > J)$. The azimuth directions of uncorrelated incident signals are $\phi_1, \phi_2, \ldots, \phi_J$. The k^{th} sample of the array output is given as:

$$\mathbf{X}[k] = \mathbf{U}[k] + \mathbf{N}[k] \tag{2.1}$$

where $\mathbf{X}[k] = \left[x_1[k], x_2[k], \ldots, x_M[k]\right]^T$, $\mathbf{U}[k] = \left[u_1[k], u_2[k], \ldots, u_M[k]\right]^T$ is the coupling-free voltage at the antenna terminal and $\mathbf{N}[k] = \left[n_1[k], n_2[k], \ldots, n_M[k]\right]^T$ is a vector of white Gaussian noise samples appearing at the antenna terminal receiver. The noise has zero mean and has correlation matrix $\sigma^2\mathbf{I}$ where σ is the standard deviation and $\mathbf{I}$ is an $M \times M$ identity matrix. The signal model in (2.1) does not consider mutual coupling within the array. Elements in a real antenna array interact with one another due to mutual coupling. The relation between actual voltage $\mathbf{V}$ at the antenna terminal and theoretical coupling free voltage $\mathbf{U}$ is given as:

$$\mathbf{ZV} = \mathbf{U} \tag{2.2}$$

where $\mathbf{Z}$ is an $M \times M$ matrix whose coefficients can be determined by electromagnetic analysis such as Method of Moments (MoM) or finite element method FEM. Thus, a more accurate signal model for the array output (2.1) is given as:

$$\mathbf{X}[k] = \mathbf{ZV}[k] + \mathbf{N}[k] \tag{2.3}$$

The zero-mean Gaussian noise in the receiver and signal generation in the farfield sources are independent processes. Therefore, the spatial covariance matrix for (2.3) is given as:

$$\mathbf{R} = E\{\mathbf{ZVV}'\mathbf{Z}'\} + \sigma^2\mathbf{I} \tag{2.4}$$

where σ^2 is the noise variance and $\mathbf{I}$ is the identity matrix. It is evident from (2.4) that correct knowledge of $\mathbf{Z}$ is pivotal in DOA estimation with minimum error. Considering array elements as monopoles, a method to find $\mathbf{Z}$ as the receiving mode mutual impedance is in the literature [17]. This method considers a monopole antenna over a high conductivity or perfect ground. However, in real world applications an antenna may be placed over a finite or low conductivity ground.

Consider an array of two $\lambda/4$-monopole antenna over an arbitrary ground as shown in Fig.

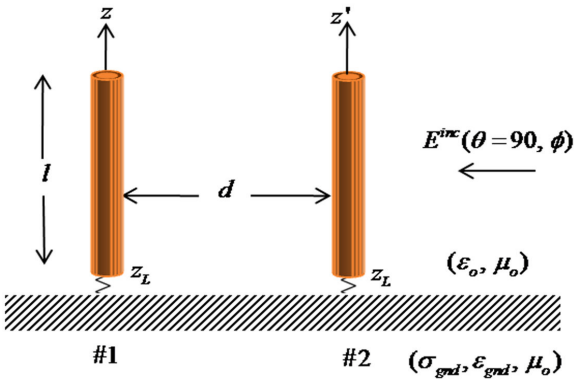

Figure 2.1: Setup for finding mutual coupling between monopole array over arbitrary ground

2.1. The array is excited by an incident plane wave and each element is connected to a load Z_L. Due to this excitation, terminal currents I_1^t and I_2^t flow in the loads of antenna # 1 and # 2, respectively. The terminal voltage at antenna terminal # 1 is given as:

$$V_1^t = I_1^t Z_L = U_1^t + W_1^t \tag{2.5}$$

where U_1^t is the voltage due the plane wave incidence alone and W_1^t is the induced voltage due the flow of current in antenna # 2. Both causes are independent of one another. Therefore,

$$W_1^t = I_2^t Z_{12} \tag{2.6}$$

where Z_{12} is the mutual impedance between element # 1 and # 2 due to the current in the load across port # 2.

Exploiting the principle of superposition, the current distribution I_1 along antenna # 1 can

be given as:

$$I_1 = I_{1U} + I_{1W} \tag{2.7}$$

where subscripts U and W correspond to the cause of the current distribution.

Therefore, the induced voltage W_1^t is given as [4]:

$$W_1^t = -\frac{1}{I_1^t}\int_0^l E_{z12}(z')I_{1w}(z')dz' \tag{2.8}$$

where $E_{z12}(z')$ is the E-field component radiated by antenna # 2 towards antenna # 1 and $I_{1w}(z')$ is the current distribution along antenna # 1. Hence, the mutual impedance in (2.5) can be given as:

$$Z_{12} = \frac{W_1}{I_2^t} = -\frac{1}{I_2^t I_1^t}\int_0^l E_{z12}(z')I_{1w}(z')dz'. \tag{2.9}$$

It is evident from equation (2.9) that for a given current I_2^t, the E-field $E_{z12}(z')$ has a major contribution in the numerical value of mutual impedance. Ideally, over a perfect ground the monopole antenna radiates strongly along the horizontal direction $\theta = 90^o$ that is towards the adjacent element in our configuration. This results in strong mutual coupling or sharing of energy between array elements. However, over a finite ground the field strength in the horizontal direction is much smaller in the near field and almost zero in the farfield [37, Chapter:23]. This reduction in field strength should reduce the mutual coupling between antenna elements placed over a finite ground.

In the next section, we will investigate this hypothesis through the FEM and present results of mutual coupling by extending the existing technique[17] to the case of finite ground and its effects on mutual coupling and DOA.

2.3 Results and Discussion

The investigation of our hypothesis is carried out by considering two $\lambda/4$-monopole antennas at 2.4 GHz as shown in Fig. 2.1. The antennas are placed over an arbitrary ground with element spacing $\lambda/2$ and are connected to a load $Z_L = 50\Omega$. The array is excited by a plane wave, whose incident direction is $(\theta = 90^o, \phi = 90^o)$. However, due to the axial symmetry of the antenna, this analysis is independent of incident azimuth direction (ϕ) for a given elevation (θ). The description of the procedure that is carried out here for finding mutual impedance is available in Appendix A.

The mutual coupling found in [17] over a wide frequency range is compared for the case when the ground plane becomes poor as given in Table 2.1; see Fig. 2.2. The result clearly shows that around the resonant frequency both the real and imaginary parts of Z_{12} over a poor ground reduces to about one third of the value of Z_{12} over a perfect ground. It is also observed that mutual coupling undergoes very small variations over a poor ground for a wide range of frequencies. This reduction of mutual impedance was motivation to investigate a wide variety of ground conditions usually encountered in

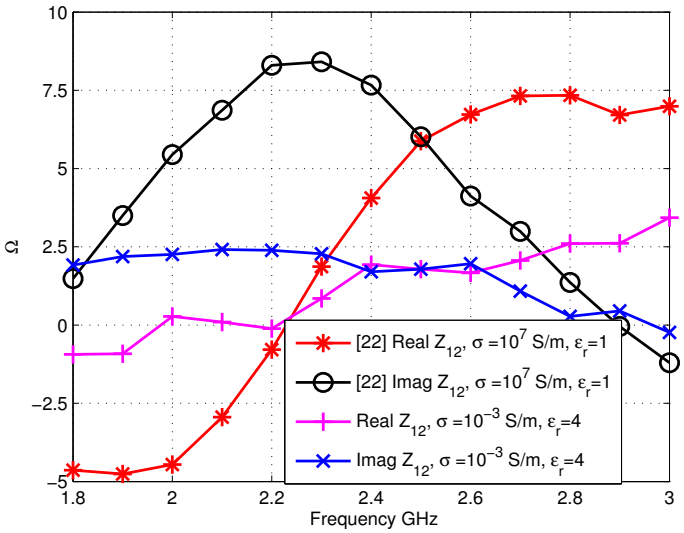

Figure 2.2: Mutual coupling between two $\lambda/4$ monopoles over poor ground and with perfect ground [17].

Table 2.1
Ground material parameters used in Fig. 2.2 [40]

Material	Relative Permittivity ε_r	Conductivity σ(S/m)
Poor Ground	4	0.001
Typical Ground	15	0.005
Good Ground	25	0.02
Sea Water	81	5.0
Fresh Water	81	0.001
Copper	1	10^7

wireless communication. Fig. 2.3 shows that even for a good electrical ground, usually made available for fixed antenna locations, the mutual coupling is still half of the value at a perfect ground. This result is expected from the fact that over a dielectric ground the monopole radiation becomes minimal along the horizontal direction and reduces the value of W_1 in (2.9). The result is consistent with the findings of [37], [38].

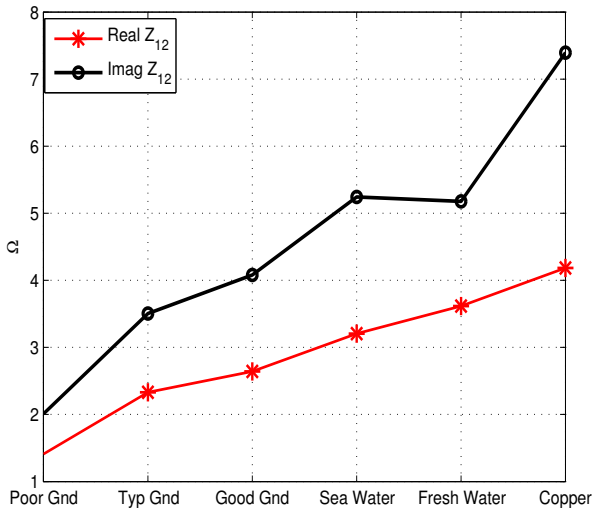

Figure 2.3: Mutual coupling between two $\lambda/4$ monopoles for various ground types at 2.4 GHz

The variation of mutual impedance over a wide range of conductivity for a nominal relative permittivity ε_r is shown in Fig. 2.4. It can be further deduced from the results that when the skin depth of the ground increases or the loss tangent decreases, the mutual impedance decreases and vice versa. We can also conclude that mutual coupling can be approximately divided between two ranges for which it assumes fairly constant values. These two ranges are when the loss tangent $\frac{\sigma}{\omega\varepsilon} \leq 1$ or $\frac{\sigma}{\omega\varepsilon} \gg 1$.

It is well known that soil water contents vary from place to place and this may result in a change of permittivity of the ground. However, this change of water content will not cause any deviation in conductivity values over a wide range of frequencies [41]. The behavior of mutual impedance for such situations is investigated and results are shown in Fig. 2.5. The curves account for variation from dry land to a saline medium such as sea water whose

$\varepsilon_r < 100$. The result depicts that for a good ground, the increase in relative permittivity increases the mutual impedance.

Table 2.2
Mutual Impedance for five element Monopole array over perfect and poor ground at 2.4 GHz

Impedance Component	Perfect Gnd [42] Ω	Perfect Gnd (FEM) Ω	Poor Gnd (FEM) Ω
$Z_{12} = Z_{21} = Z_{23} = Z_{32} = Z_{34} = Z_{43} = Z_{45} = Z_{54}$	4.0 + j8.7	4.1 + j8.2	1.4 + j2.0
$Z_{13} = Z_{31} = Z_{24} = Z_{42} = Z_{35} = Z_{53}$	-1.3 - j5.2	-1.3 - j5.6	0.3 - j1.1
$Z_{14} = Z_{41} = Z_{25} = Z_{52}$	0.7 + j3.6	0.8 + j2.7	-0.03 + j0.13
$Z_{15} = Z_{51}$	-0.4 - j 2.7	-0.8 - j2.0	0.07 - j0.27

Investigation of the effects of arbitrary ground mutual coupling on DOA estimation is carried out by simulation. An array of five vertical quarter wave monopoles is taken as the DOA estimator antenna, the spacing between elements is $\lambda/2$ and the array is operating at 2.4 GHz. The mutual coupling matrix **Z** is calculated according to [17] by placing antennas

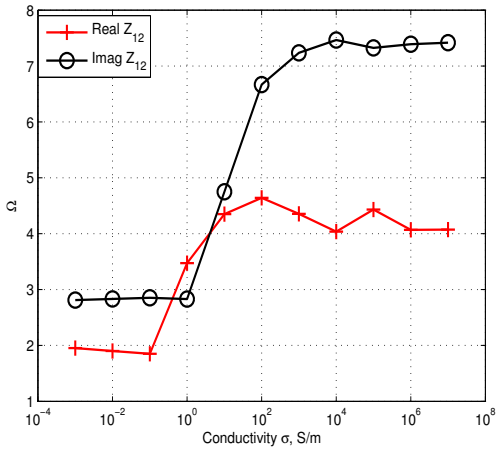

Figure 2.4: Mutual coupling between two $\lambda/4$ monopoles at 2.4 GHz for $\sigma = 10^{-3}$ to 10^{7} S/m, ε_r=10

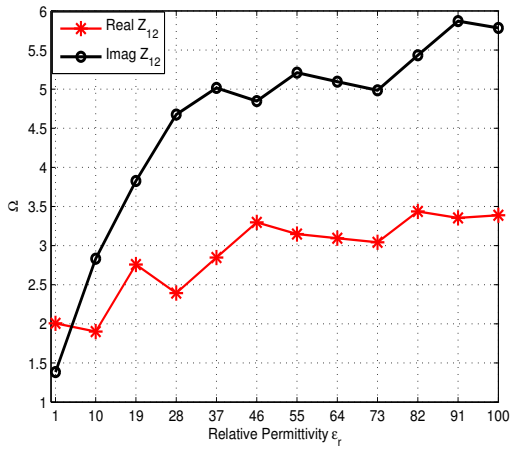

Figure 2.5: Mutual coupling between two $\lambda/4$ monopoles at 2.4 GHz for ε_r =1 to 100, σ=0.02 S/m

over a poor and a perfect ground, respectively. The mutual impedances are given in Table 2.2 whose second column contains values from [42]. DOA estimation is carried out for a vertically polarized farfield source at $\theta = 90^o, \phi = 90^o$. The terminal voltage vector $\mathbf{V}$ at the antenna ports is found in the COMSOL® multiphysics environment [43], for a terminal load of 50Ω. The effect of mutual coupling on the terminal voltage vector $\mathbf{V}$ is removed and the coupling free voltage vector $\mathbf{U}$ is found by using (2.2). At SNR=40 dB, white Gaussian noise is added to the coupling-free terminal voltage. The covariance matrix is found by (2.4) and the MUSIC algorithm [9] is used to estimate azimuth (ϕ) of the incident source. The root mean square error (RMSE) for 1000 Monte-Carlo simulations is calculated each for poor and perfect ground conditions.

Table 2.3 shows RMSE in DOA estimation for three different cases. Case #1 shows the RMSE when the antenna is over perfect ground and effects of mutual coupling is removed by using mutual impedance matrix measured over the same ground condition. The RMSE

Table 2.3
RMSE of DOA estimation for array for perfect and poor ground

Case #	Type of Ground for DOA Estimation	Type of Ground for **Z** Estimation	RMSE Degrees
1	Perfect ground	Perfect Ground / Copper	0.01
2	Poor ground	Perfect Ground / Copper	1.6
3	Poor ground	Poor Ground	0.03

is fairly low, which supports the applicability of the method presented in [44]. The critical situation arises when the antenna is placed over a poor ground and the mutual impedance matrix is pre-estimated over a perfect ground. Now if we try to remove mutual coupling effects from the measured terminal voltages by using this pre-estimated mutual impedance matrix according to (2.2), the result worsens as shown by a higher RMSE for case #2. The significant increase in RMSE shows that the mutual impedance matrix estimated in [42] over perfect ground is not able to sufficiently remove errors in DOA estimation for the case when the antenna is placed over poor ground. The obvious solution to this problem is to estimate actual mutual impedances over poor ground as shown in the fourth column of Table 2.2, then use it as in (2.2) for DOA estimation. The resultant RMSE (case #3) is very close to the result found for case #1 where the antenna placement for DOA estimation and **Z** matrix calculation were both carried out for perfect ground. The argument here is that mobile or portable antennas encounter a variety of ground situations and in these scenarios the pre-estimated mutual impedance matrix for an ideal case of perfect ground can not be used to fully remove the errors in DOA estimation. Thus, if the situation permits, one should measure the actual mutual impedance values for the given ground condition before

estimating DOAs. However, a universal solution to this problem that works equally well for all ground conditions is still an open problem.

2.4 Conclusion

This chapter investigated the effects of ground parameters on mutual impedance for DOA estimation. To the best of the authors' knowledge these results are novel and extend the application of an existing technique [17] to real-earth situations. Significant impact of ground constituent parameters on mutual impedance is observed. As a rule of thumb, for applications on a real earth, the authors suggest reducing the values of mutual impedance between two vertical monopoles to 50% of the values found in the anechoic chamber over a perfect ground. The increase of RMSE in cases where the antenna is placed over poor ground and pre-estimated mutual impedance matrix (assuming perfect ground) is used to remove errors in DOA underscores the importance of this research. The authors propose that the technique of estimating mutual coupling presented in [17] is applicable to all ground conditions, provided the antennas be placed on the respective grounds. It is understood that it is not always possible to pre-estimate mutual impedance for a variety of ground conditions. It is also worth noting that most of the DOA estimation techniques in the literature assume the array is in free space. Therefore, this research also motivates the need for a universal solution of this issue that can be used for any arbitrary ground condition. The authors wish to continue this work to find effects of ground parameters on

other commonly used antenna elements when they are placed near ground. In Chapter 3, the authors continue with the investigation and find effects of antenna height and certain polarization on the mutual coupling of the half wave dipole array.

Chapter 3

Effects of Ground on Antenna Mutual Impedance for DOA Estimation Using Dipole Arrays*

3.1 Introduction

There is a growing interest in the wireless community to broaden the source localization capability of the devices. Global position system (GPS) or devices attached to a cellular network are already providing this facility with a certain accuracy. However, where satellite

*Parts of this chapter have been submitted for publication in IET *Electronics Letters*.

signals cannot be employed or where independent portable networks are to be deployed, locating physical coordinates of a wireless source is a local direction finding problem. Several methods such as received-signal-strength (RSS) [45], time-of-arrival (TOA) [46], time-difference-of-arrival (TDOA) [47], and direction-of-arrival (DOA) [12] are in the literature for finding the direction of a radio source. Traditionally, DOA techniques exploit the antenna array structure properties to estimate direction of incident signals. Antenna arrays consist of collocated antenna elements that are uniformly or non-uniformly distributed [4], [5]. Usually, for simplicity of synthesis, all driven elements in an array are kept identical. The performance of antenna arrays is severely compromised due to the mutual coupling between elements, proximity of scatterers, and operating at low altitude near real-earth. [48, p. 30.56]. Antenna mutual coupling is one phenomenon that introduces significant errors in DOA estimation [15].

A number of authors proposed techniques to counter errors in DOA estimation due to the mutual coupling [15] [18], [24], [17], [25]. In general, these techniques do not consider the interaction of the antenna array with an imperfect ground in the near-zone [36]. Effects of ground proximity and constituent parameters on wire antennas have been presented in the literature [37], [38], [39]. Relation of ground constituent parameters with mutual impedance between two wire loop antennas has also been investigated [49]. Recently, effects of ground constituent parameters on received mutual coupling of monopole array for DOA estimation have also been reported [34]. To the authors' knowledge, investigation of received mutual coupling of dipole array for DOA estimation near real-earth is still an

open problem.

This chapter considers the effects of ground on the mutual coupling of an array of dipoles and impact on DOA estimation. Numerical values of received mutual coupling of a dipole array for DOA estimation are in the literature [50]. The operating environment for [50] is presumably free-space. However, the real-ground or earth has finite conductivity and may have high permittivity which are certain to have an impact on mutual coupling. The effects of antenna height and polarization in conjunction to ground conductivity on mutual coupling is investigated. The evaluation of mutual coupling is an extension of the technique [17] to the near-ground case. The newly-found mutual coupling is used to compensate errors in DOA estimation for an array over a good-ground.

3.2 Problem Formulation

The nature of the problem formulation for this chapter is similar to section 2.2 except that instead of a monopole antenna , the element under consideration is a $\lambda/2-$dipole antenna. In Section 2.2 a uniform linear array (ULA) of M omnidirectional elements is considered for DOA estimation. It is supposed that plane waves from J narrowband farfield sources are incident on this array and $(M > J)$. The azimuth directions of uncorrelated incident signals are $\phi_1, \phi_2, \ldots, \phi_J$. The k^{th} sample of the array output; as given by (2.3), is:

$$\mathbf{X}[k] = \mathbf{Z}\mathbf{V}[k] + \mathbf{N}[k] \tag{3.1}$$

where $\mathbf{X}[k] = \left[x_1[k], x_2[k], \ldots, x_M[k]\right]^T$, $\mathbf{V}[k] = \left[v_1[k], v_2[k], \ldots, v_M[k]\right]^T$ is the measured voltage at the antenna terminal and $\mathbf{N}[k] = \left[n_1[k], n_2[k], \ldots, n_M[k]\right]^T$ is a vector of white Gaussian noise samples appearing at the antenna terminal receiver. The noise has zero mean and has correlation matrix $\sigma^2\mathbf{I}$ where σ is the standard deviation and $\mathbf{I}$ is an $M \times M$ identity matrix where $\mathbf{Z}$ is an $M \times M$ matrix complex coefficients. The spatial covariance matrix for (3.1) is given by (2.4) as:

$$\mathbf{R} = E\{\mathbf{Z}\mathbf{V}\mathbf{V}'\mathbf{Z}'\} + \sigma^2\mathbf{I} \tag{3.2}$$

where σ^2 is the noise variance and $\mathbf{I}$ is the identity matrix. It is evident from (3.2) that correct knowledge of $\mathbf{Z}$ is pivotal in DOA estimation with minimum error. With the $\lambda/2$-dipole antenna as the array element, a method to find $\mathbf{Z}$ as the receiving mode mutual impedance is in the literature [17]. A similar approach is also used to find mutual impedance between elements of $\lambda/2$-dipole array acting as a receiver in the free-space [50].

Consider an array of two $\lambda/2$-dipole antennas over an arbitrary ground as shown in Fig.3.1. The array is excited by an incident plane wave and each element is connected to a load Z_L. Due to this excitation, terminal currents I_1^t and I_2^t flow in the loads of antenna # 1 and # 2,

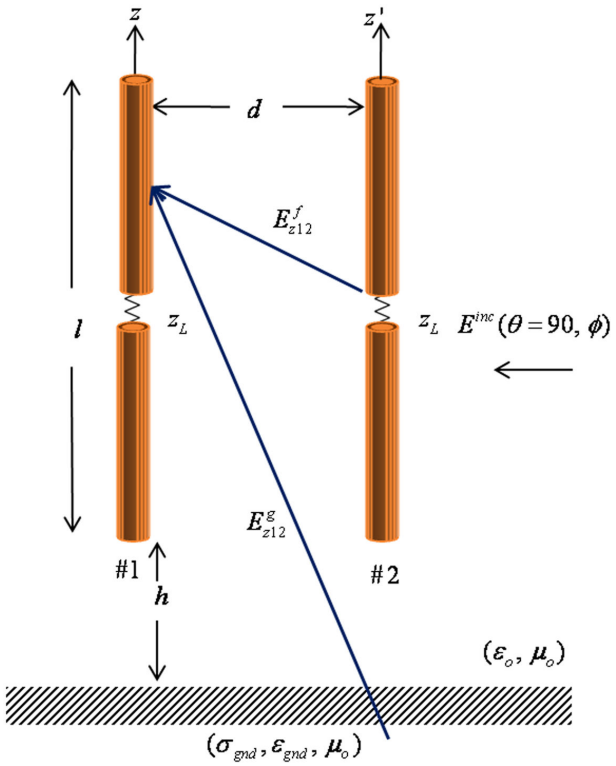

Figure 3.1: Setup for finding mutual coupling between vertical dipole array over arbitrary ground

respectively. The mutual impedance between this pair of dipoles is defined by (2.9) as:

$$Z_{12} = \frac{W_1}{I_2^t} = -\frac{1}{I_2^t I_1^t} \int_0^l E_{z12}(z') I_{1w}(z') dz' \tag{3.3}$$

where the notations have similar meanings as defined by the equations (2.5), (2.7), and (2.8).

It is evident from equation (3.3) that for a given current I_2^t, the E-field $E_{z12}(z')$ has a major contribution in the numerical value of mutual impedance. However, in the presence of an arbitrary ground in the proximity of the antenna, the electric field E_{z12} is deeply affected

and can be divided in two components as following [51]:

$$E_{z12} = E^{f}_{z12} + E^{g}_{z12} \tag{3.4}$$

where E^{f}_{z12} is the component of the field as if it is in free-space, while E^{g}_{z12} is due to the image of the element in the ground. In general, due to the complexity of the problem, the analytical solution of (3.4) cannot be found [38].

The investigation of effects of ground conductivity with a certain antenna height revealed that nearly after a height of half wavelength, the driving point impedance of a vertical dipole becomes independent of ground conductivity [38]. We hypothesize that a result of similar nature should appear for the antenna mutual coupling of dipole arrays over arbitrary ground conductivity for height greater than a half wavelength. In the next section, we will investigate this hypothesis through the FEM and present results of mutual coupling by extending the existing technique [17] to the case of finite ground and its effects on mutual coupling and DOA. Effects of height for horizontal and vertical polarization on the mutual coupling of a dipole array and subsequent effects on DOA are also investigated.

3.3 Results and Discussion

In this section, the mutual impedance of a dipole array over a variety of ground conductivities and antenna heights is investigated. It is well known that the mutual coupling of wire type arrays is independent of direction of azimuth incidence (ϕ) for a given elevation (θ). The investigation is carried out each for vertical and horizontal antennas receiving corresponding vertically and horizontally polarized waves. The description of procedure for the estimation of mutual impedance ia available as Appendix A.

3.3.1 Vertical Polarization

Consider two $\lambda/2$ dipole antennas at 2.4 GHz as shown in Fig.3.1. The antennas are placed over a finite ground with element spacing $\lambda/2$ and are connected to a load $Z_L = 50\Omega$. The array is excited by a vertically polarized plane wave, whose incident direction is ($\theta = 90^o, \phi = 90^o$).

The mutual impedance is found for a range of antenna heights $h = 0 \ to \ 10\lambda$ from a ground having fixed permittivity $\varepsilon_r = 1$ and varied conductivity as shown in Fig.3.2. Except for the case when ground conductivity is similar to a perfect conductor $\sigma = 10^7 S/m$, mutual impedance values remain identical to each other for both very poorly conductive ground

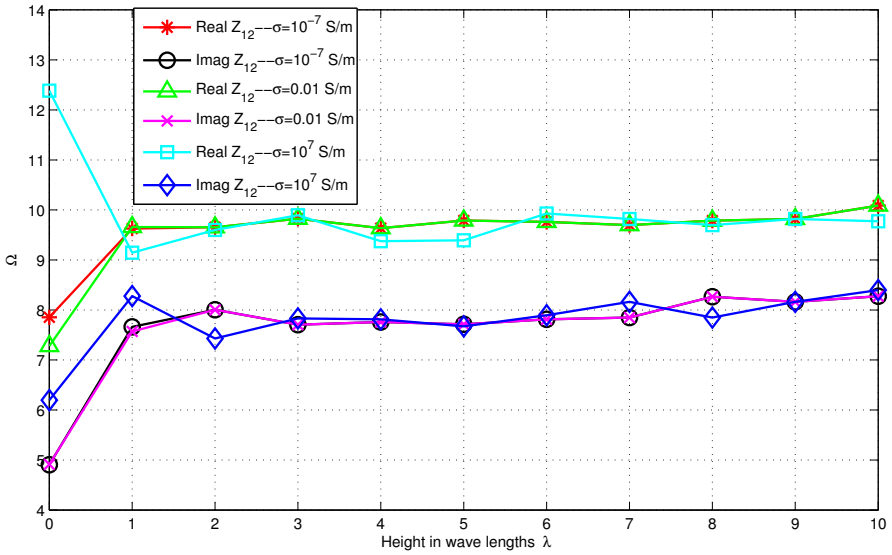

Figure 3.2: Mutual impedance between two $\lambda/2$ vertical dipoles over ground, various σ and antenna heights

$\sigma = 10^{-7} S/m$ and for a typical good ground $\sigma = 0.01 S/m$. However, for $h \geq \lambda$, mutual impedance values over high conductivity ground start aligning with real-earth values. It is also observed from Fig.3.2 that both the real and imaginary values of mutual impedance become roughly independent of ground conductivity once the antenna is placed at a height $h \geq \lambda$. The height is measured from the bottom tip of the dipole antenna.

A more detailed result of mutual impedance for given ground conductivities when an antenna is placed very near to the ground $0 < h \leq \lambda$ is shown in Fig.3.3. There are variations in the values of mutual impedance for the case when conductivity is close to perfect ground. However, it can be concluded that for an antenna height $h \geq 0.25\lambda$ mutual impedance becomes independent of the presence of conductivities found in real-earth. The result is consistent with the findings in [38], which showed independence of antenna driving

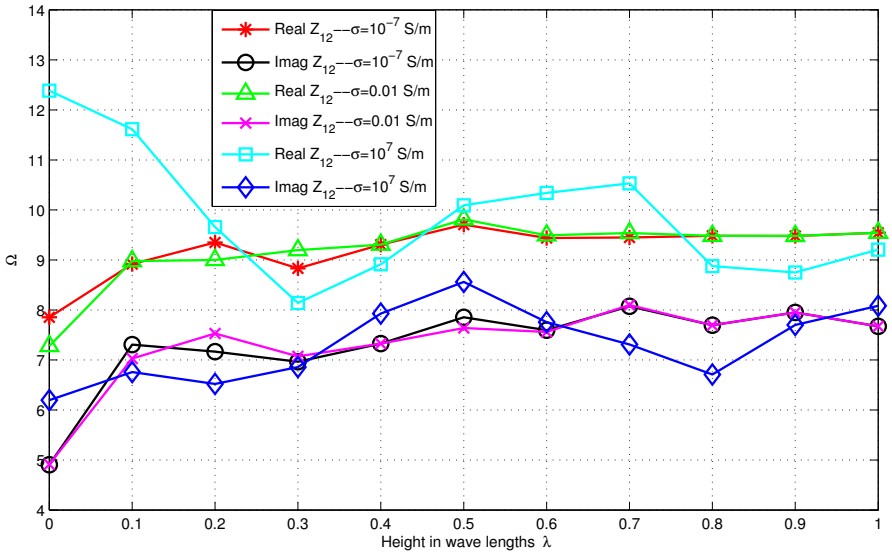

Figure 3.3: Mutual impedance between two $\lambda/2$ vertical dipoles over ground, exploded image of Fig.3.2 for $0 < h < \lambda$

point impedance from typical ground conductivities for antenna height $h \geq 0.2\lambda$.

3.3.2 Horizontal Polarization

Consider $\lambda/2$-dipole antennas at 2.4 GHz parallel to the xy plane with the axis of antenna elements directed along y-axis as shown in Fig.3.4. The antennas are placed over a finite ground with element spacing $\lambda/2$ and are connected to a load $Z_L = 50\Omega$. The array is excited by a horizontally polarized plane wave, whose incident direction is $(\theta = 90^o, \phi = 90^o)$. The antenna height is measured along the z-axis.

The variation of mutual impedance for a wide range of antenna heights over ground having

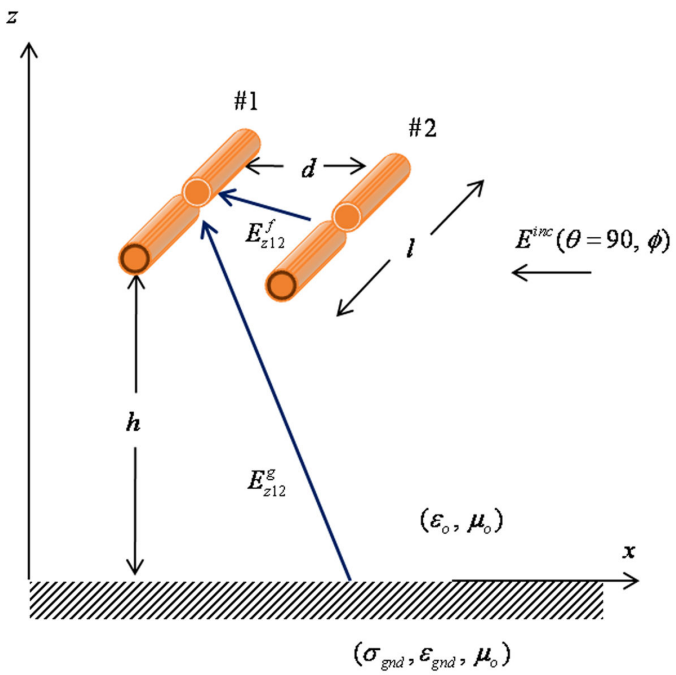

Figure 3.4: Setup for finding mutual coupling between horizontal dipole array over arbitrary ground

relative permittivity $\varepsilon_r = 1$ and various conductivities is shown in Fig.3.5. It can be deduced from the results that sensitivity to antenna height for horizontal polarization is similar to vertical polarization for $h \geq \lambda$. For the purpose of mutual impedance estimation, one can cautiously divide the antenna height regions into two parts: very near ground $h < \lambda$ and fairly free-space $h \geq \lambda$. In Fig.3.6 the antenna height region $0 \leq h \leq \lambda$ is shown in magnified form. Unlike vertical polarization, the variations in mutual impedance values is significant for the conductivity nearly equal to a perfect conductor. This is tantamount to the ground acting as a scatterer of conducting material because a horizontally polarized wave excites current in the ground. However, for low values of conductivity, the mutual impedance suffers very minor variations due to the changes in conductivity when antenna height $h \geq 0.25\lambda$. The increase in insensitivity of driving point impedance to ground

conductivity variations after attaining an antenna height $h = 0.5\lambda$ is presented in [52].

3.3.3 Effects on DOA Estimation

Investigation of the effects of antenna height from a good ground ($\varepsilon_r = 1, \sigma = 0.01 S/m$) on mutual coupling for DOA estimation is carried out by simulation. An array of four vertical half wave dipoles is i the DOA estimator antenna, and the spacing between elements is $\lambda/2$ at 2.4 GHz. The mutual coupling matrix $\mathbf{Z}$ is calculated according to [17] by placing antennas over $h = 0.25\lambda$ and $h = 10\lambda$, respectively. DOA estimation is carried out for a vertically polarized farfield source at $\theta = 90^o, \phi = 90^o$. The terminal voltage vector $\mathbf{V}$ at the antenna ports is measured in the COMSOL® multiphysics environment [43], for

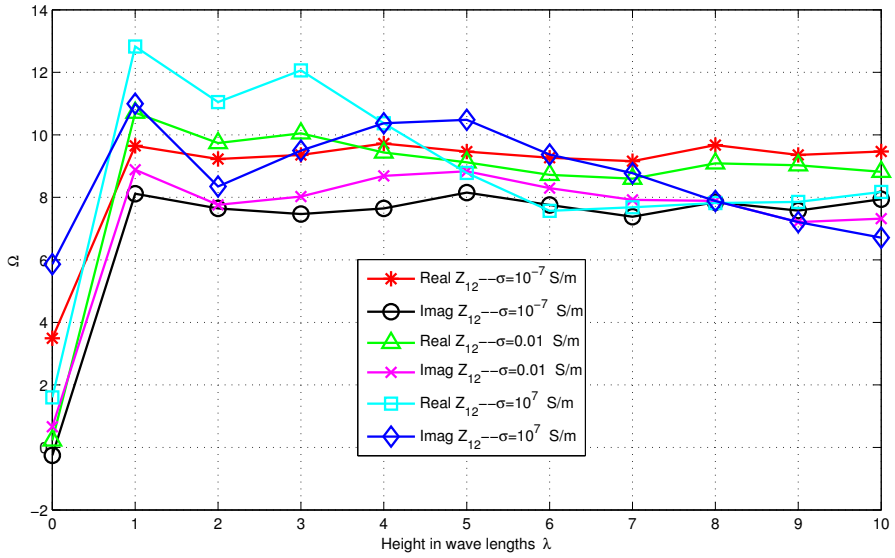

Figure 3.5: Mutual impedance between two $\lambda/2$ horizontal dipoles over ground, various σ and antenna heights

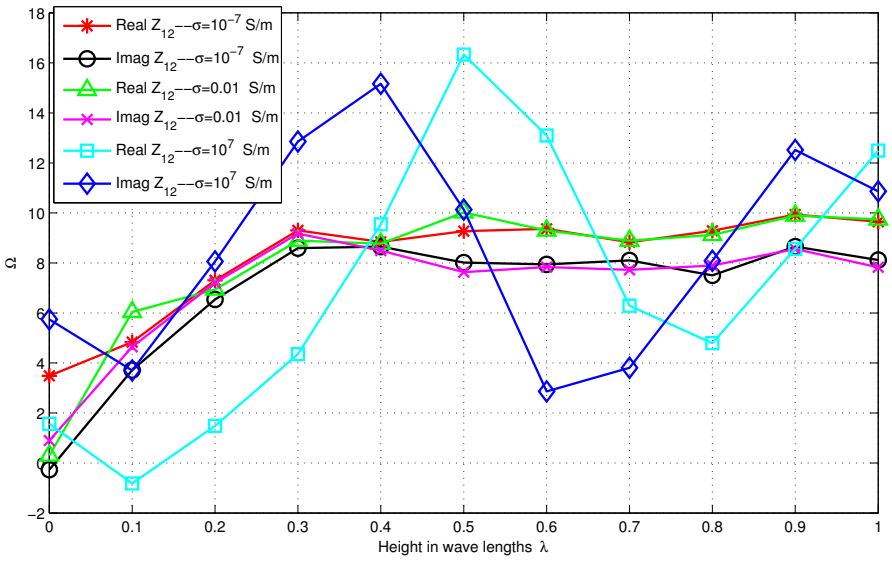

Figure 3.6: Mutual impedance between two $\lambda/2$ horizontal dipoles over ground, exploded image of Fig.3.5 for $0 < h < \lambda$

a terminal load of 50Ω. The effect of mutual coupling on the terminal voltage vector $\mathbf{V}$ is removed and coupling free voltage vector $\mathbf{U}$ is found by using $\mathbf{ZV} = \mathbf{U}$. At SNR=30 dB, white gaussian noise is added to the coupling-free terminal voltage. The covariance matrix is found by (3.2) and the MUSIC algorithm [9] is used to estimate azimuth (ϕ) of the incident source. Root mean square error (RMSE) for 1000 Monte-Carlo simulations is calculated each for poor and perfect ground conditions.

Table 3.1 shows RMSE in DOA estimation for three different cases. Case #1 shows the

Table 3.1
RMSE of DOA estimation for certain antenna heights from a good ground

Case #	Antenna Height for DOA Estimation	Antenna Height for **Z** Estimation	RMSE Degrees
1	10λ	10λ	0.06
2	0.25λ	10λ	0.06
3	0.25λ	0.25λ	0.06

RMSE when the antenna is at $h = 10\lambda$ and we remove mutual coupling effects by using a mutual impedance matrix measured over the same height. The RMSE is fairly low, which supports the applicability of the method presented in [44]. The critical situation is tested when the antenna is placed at $h = 0.25\lambda$ and the mutual impedance matrix is pre-estimated over $h = 10\lambda$, but surprisingly RMSE remains unchanged. The vertically polarized incident wave does not cause significant currents in the real-earth, so the MUSIC algorithm was able to cope with the minor voltage perturbation after removing the mutual coupling. In case #3 both DOA and mutual impedance estimation is carried out at $h = 0.25\lambda$. Case #3 supports this conclusion that the existing method [42] of removing mutual coupling for azimuth DOA estimation is valid for the near ground case using dipole arrays. However, where monopole arrays are used, effects of real-ground parameters are significant on DOA estimation because monopoles need perfect ground for exploitation of image theory [34].

3.4 Conclusion

This research investigated the effects of ground conductivity on mutual impedance for DOA estimation using dipole arrays. To the best of authors' knowledge, these results are novel and support the application of an existing technique [17] to real-earth situations. The antenna mutual impedance showed insensitivity to the ground conductivity for antenna height $h \geq \lambda$. The invariance of RMSE of DOA estimation to antenna height measured from a typical good-ground suppresses concerns in using the existing method for

removing received mutual coupling effects on DOA estimation near real-ground. However, this research has not investigated inclined incidence, variation in permittivity and other available incident polarizations, so these are some of the possible offshoots.

Chapter 4

Direction Finding in the Presence of Near-Zone Resonant Size Scatterers*

4.1 Introduction

Wireless devices with the capability of direction-of-arrival estimation (DOA) have many applications such as command and control, security and safety, and MIMO communication. Several techniques have been developed and presented in the literature to estimate DOA [8]. In general, these methods assume that the antenna elements are ideal and operate in free space. The real-world problem is totally different where antenna elements share energy

*Parts of this chapter have been submitted for publication in *International Journal of Electronics and Communications*. The publisher allows the authors to use their articles in dissertations [53].

with themselves, known as mutual coupling. Moreover, the presence of scatterers in the vicinity of antenna results in distortion of the signal and causes DOA estimation error[21].

A number of researchers' proposed methods compensate for the effects of mutual coupling for real antenna elements [15], [35], [18], [17], [24], [25]. These techniques proved effective in significant reduction of errors in DOA estimation for an array operating in an environment similar to free space. Thus, the presence of any near-zone scatterer is ignored or not considered in the signal model. These methods also assume that sources are in the farfield and, therefore, incident waves are plane waves. However, any scatterer in the near-zone produces spherical waves when illuminated by farfield sources [23]. The plane waves from the farfield are desired signals, and spherical waves due to near-zone scattering are the interfering signals.

In the last decade, some authors addressed the joint problem of mutual coupling and near-zone scatterers, by techniques whose essence is offline calibration [21], [22], [31]. Fewer antenna elements are required by transforming the non-uniform array to a virtual uniform array to find DOA in an environment for which steering vectors are previously measured/computed [21]. Non-conventional least squares optimization is used to exploit the large data set of pre-calibrated steering vectors for DOA estimation with near-zone scatterers [22]. The square calibration matrix of [18] is proposed as non-square to address the scattering from a known scatterer or platform structure [31]. These methods are suitable for fixed antenna where the environment remains stationary. However, when either antenna

is portable or the environment is not stationary, these methods will yield errors and require re-calibration, which is not convenient for many applications.

One way to address the issue of portable antenna where pre-calibration cannot last long is self- or auto-calibration. The auto-calibration techniques exploit the signals from the sources of opportunity to sufficiently remove errors in the DOA estimate, while estimating the DOA simultaneously. Thus, no additional source is required to calibrate the array. A self-calibration technique for DOA estimation using the MUSIC algorithm where an uncoupled near-field scatterer is present is given in [23]. This method does not remove the effects of mutual coupling and works only for 2D scatterers. A self calibration algorithm that removes the effects of mutual coupling and near-zone scatterer is also in the literature [32]. This algorithm approximates a scatterer as a cylinder and, therefore, assumes cylindrical harmonic expansion origination in response to a plane wave incidence. The algorithm is iterative and does not guarantee convergence to the true DOA. It also works only for 2D scatterers and requires a large number of antenna elements.

In a real-world 3D environment, a finite-size scatterer is more accurately modeled as a sphere, and as stated by [23] produces spherical harmonics in response to plane wave excitation. This chapter extends the iterative algorithm approach presented in [32] to a 3D case where scatterers are modeled as a sphere and the algorithm utilizes spherical harmonic expansion. Although like its predecessor, a solution is not guaranteed, but convergence is achieved with far fewer antenna elements. It is highly likely that the presence of

near-zone scatterers results in spurious peaks in the DOA spectrum which cause errors in the initial estimate of the number of sources [22, Fig 14]. This issue of spurious number of sources was not explicitly described in [32]. Our algorithm suppresses the spurious peaks and corrects the detection of the number of sources in addition to the removal of DOA estimation errors. Classical DOA estimation methods [54], [2] are incorporated in this algorithm. The algorithm estimates elevation θ_l of incident sources present in the farfield.

Section 4.2 will describe the method and explain the algorithm. Numerical examples showing capability of the method for a variety of complexities are presented in Section 4.3. Section 4.4 concludes the chapter and Section 4.5 provides symbol definitions and nomenclature.

4.2 Method Description

4.2.1 Problem Statement

To illustrate the problem, consider TM_x plane waves incident on an antenna array of x-directed thin wires. All currents and fields in the antenna elements are also x-directed. Fig.4.1 shows the problem setup where a field is incident on an antenna array of M elements, and the location of mth element is $\mathbf{r}_m = (x_m, y_m, z_m)$. The scatterer's location $\mathbf{r}_s = (x_s, y_s, z_s)$ is known, but its geometry is unknown. It is also assumed that the antenna

and environment is stationary during DOA estimation.

The total field at the mth antenna element is given as the sum of the incident and scattered field (from spherical scatterer)

$$\mathbf{E}^t = \mathbf{E}^{inc} + \mathbf{E}^{sct} \tag{4.1}$$

The x-directed incident field at the mth antenna element due to L incident waves is given as

$$E_m^{inc}(x) = \sum_{l=1}^{L} E_l E_m^{PW}(\theta_l, \phi_l) = \sum_{l=1}^{L} E_l e^{j\beta(x_m sin\theta_l cos\phi_l + y_m sin\theta_l sin\phi_l + z_m cos\theta_l)} |E_m^{inc}(x)| \tag{4.2}$$

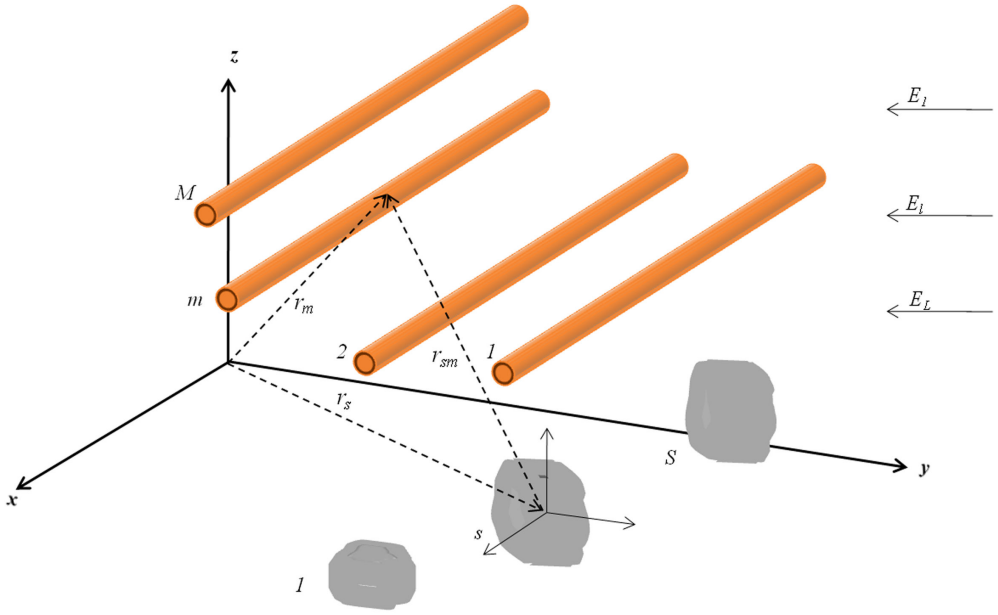

Figure 4.1: Incident plane wave on M element array with spherical scatterer

When a sphere is excited by a TM_x plane wave, the corresponding spherical harmonic expansion is in [55]. Letting the magnitude $|E_m^{inc}(x)| = E_o$, the scattered field along the x-axis at the mth antenna element due to S spherical scatterers at known locations in the near-zone is given as:

$$\begin{aligned} E_m^{sct}(x) \quad = \quad & \sum_{s=1}^{S}\Bigg[(sin\theta_{sm}cos\phi_{sm})\Big[-jE_o cos\phi_{sm}\sum_{q=1}^{\infty} b_{sq}\big[\hat{H}_{sq}^{(2)''}(\beta r_{sm})+\hat{H}_{sq}^{(2)}(\beta r_{sm})\big]P_{sq}^{1}(cos\theta_{sm})\Big] \\ & +(cos\theta_{sm}cos\phi_{sm})\Big[\frac{E_o}{\beta r_{sm}}cos\phi_{sm}\sum_{q=1}^{\infty}\big[jb_{sq}\hat{H}_{sq}^{(2)'}(\beta r_{sm})sin\theta_{sm}P_{sq}^{'1}(cos\theta_{sm})-c_{sq}\hat{H}_{sq}^{(2)}(\beta r_{sm})\frac{P_{sq}^{1}(cos\theta_{sm})}{sin\theta_{sm}}\big]\Big] \\ & +(-sin\phi_{sm})\Big[\frac{E_o}{\beta r_{sm}}sin\phi_{sm}\sum_{q=1}^{\infty}\big[jb_{sq}\hat{H}_{sq}^{(2)'}(\beta r_{sm})\frac{P_{sq}^{1}(cos\theta_{sm})}{sin\theta_{sm}}-c_{sq}\hat{H}_{sq}^{(2)}(\beta r_{sm})sin\theta_{sm}P_{sq}^{'1}(cos\theta_{sm})\big]\Big]\Bigg]. \end{aligned} \tag{4.3}$$

To make the equation concise, the following constants can be introduced for a fixed geometrical location

$$U_{sm} = -jsin\theta_{sm}cos^2\phi_{sm} \tag{4.4}$$

$$V_{sm} = \frac{cos\theta_{sm}cos^2\phi_{sm}}{\beta r_{sm}} \tag{4.5}$$

$$W_{sm} = \frac{-sin^2\phi_{sm}}{\beta r_{sm}}. \tag{4.6}$$

The individual estimation of source amplitude E_o that excited the scatterers is not our concern, so we merged it with unknown amplitudes of the harmonics to form two new unknown amplitudes as following:

$$B_{sq} = E_o b_{sq} \tag{4.7}$$

$$C_{sq} = E_o c_{sq} \tag{4.8}$$

The five harmonic forms (indexed in superscript) can be written as:

$$G^1_{sqm} = \left[\hat{H}^{(2)''}_{sq}(\beta r_{sm}) + \hat{H}^{(2)}_{sq}(\beta r_{sm})\right] P^1_{sq}(cos\theta_{sm})\Big] \tag{4.9}$$

$$G^2_{sqm} = j\hat{H}^{(2)'}_{sq}(\beta r_{sm}) sin\theta_{sm} P'^1_{sq}(cos\theta_{sm}) \tag{4.10}$$

$$G^3_{sqm} = \hat{H}^{(2)}_{sq}(\beta r_{sm}) \frac{P^1_{sq}(cos\theta_{sm})}{sin\theta_{sm}} \tag{4.11}$$

$$G^4_{sqm} = j\hat{H}^{(2)'}_{sq}(\beta r_{sm}) \frac{P^1_{sq}(cos\theta_{sm})}{sin\theta_{sm}} \tag{4.12}$$

$$G^5_{sqm} = \hat{H}^{(2)}_{sq}(\beta r_{sm}) sin\theta_{sm} P'^1_{sq}(cos\theta_{sm}) \tag{4.13}$$

.

Therefore, equation (4.3) can be given in the form of known harmonics and their unknown amplitudes as following:

$$E^{sct}_m(x) = \sum_{s=1}^{S} \left[U_{sm} \sum_{q=1}^{Q} B_{sq} G^1_{sqm} + V_{sm} \sum_{q=1}^{Q} [B_{sq} G^2_{sqm} - C_{sq} G^3_{sqm}] + W_{sm} \sum_{q=1}^{Q} [B_{sq} G^4_{sqm} - C_{sq} G^5_{sqm}] \right]. \tag{4.14}$$

Note that we are not determining the current density on the scatterer as it is not needed for

our method. Suppose our receiver is capable of measuring total voltage at the m_{th} antenna terminal V_m^t. The total voltage received at an antenna terminal can be expressed as the following:

$$V_m^t = V_m^{inc} + V_m^{sct} \tag{4.15}$$

where at the m_{th} antenna terminal V_m^i is the voltage due to the incident filed $E_m^{inc}(x)$ alone and V_m^{sct} is the voltage due to scattered field arising from near-zone scatterers $E_m^{sct}(x)$.

4.2.2 Solution

As mentioned earlier, the total voltage at the antenna terminal is measured or known. The flow diagram of the iterative technique to determine DOA by finding V^{inc} and V^{sct} from the knowledge of V^t is shown in Fig. 4.2. The algorithm removes the effects of mutual coupling in an implicit way by forcing V^{inc} to be a coupling free voltage vector, while putting all the perturbations in the V^{sct} vector. In the absence of any scatterer, the environment can be considered as free space and V_m^t suffers perturbation due to mutual coupling between elements only. In this special case ($S = 0$), any of the available methods [15], [35], [18], [17], [24], [25] can be embedded into this proposed iterative algorithm. The index of iteration $k = 0, 1, 2, ..., K$ is used in the superscript of unknown parameters described in the

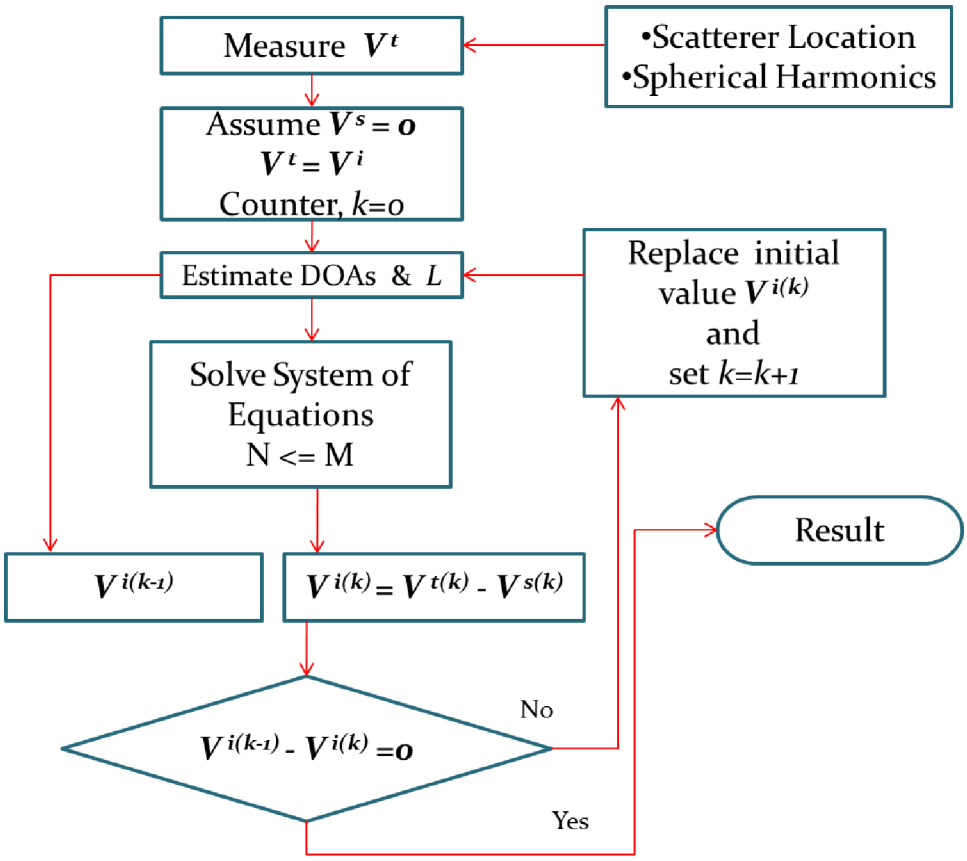

Figure 4.2: Flow diagram of the iterative algorithm

previous section. At convergence, the iteration index is K. The following steps describe the algorithm:

1. Given that the V^t is known and initially assumed as the desired V^{inc} voltage, and classical DOA estimation techniques are also available [3], [2]. At $k = 0$ the iteration estimates the number of sources $L^{(k)}$ and their elevation $\theta = [\theta_1^{(k)}, \theta_2^{(k)}, ..., \theta_L^{(k)}])$. It is to be noted that the incorrect assumption of letting $V^t = V^{inc}$ not only causes errors in the DOA estimate but may also gives rise to spurious peaks in the DOA spectrum [22]. Thus, the initial estimate of number of sources may be higher than actual.

2. Having the number of sources and DOA estimates from step 1, (4.15) for an array of M elements can be written as set of M simultaneous linear equations.

$$\begin{bmatrix} V_1^t \\ V_2^t \\ \vdots \\ V_m^t \\ \vdots \\ V_M^t \end{bmatrix} = \begin{bmatrix} \sum_{l=1}^{L} E_1^{PW}(\theta_l,\phi_l) & \sum_{s=1}^{S}\sum_{q=1}^{Q}[U_{s1}G_{sq1}^1 + V_{s1}G_{sq1}^2 + W_{s1}G_{sq1}^4] & \sum_{s=1}^{S}\sum_{q=1}^{Q}[-V_{s1}G_{sq1}^3 - W_{s1}G_{sq1}^5] \\ \sum_{l=1}^{L} E_2^{PW}(\theta_l,\phi_l) & \sum_{s=1}^{S}\sum_{q=1}^{Q}[U_{s2}G_{sq2}^1 + V_{s2}G_{sq2}^2 + W_{s2}G_{sq2}^4] & \sum_{s=1}^{S}\sum_{q=1}^{Q}[-V_{s2}G_{sq2}^3 - W_{s2}G_{sq2}^5] \\ \vdots & & \\ \sum_{l=1}^{L} E_m^{PW}(\theta_l,\phi_l) & \sum_{s=1}^{S}\sum_{q=1}^{Q}[U_{sm}G_{sqm}^1 + V_{sm}G_{sqm}^2 + W_{sm}G_{sqm}^4] & \sum_{s=1}^{S}\sum_{q=1}^{Q}[-V_{sm}G_{sqm}^3 - W_{sm}G_{sqm}^5] \\ \vdots & & \\ \sum_{l=1}^{L} E_M^{PW}(\theta_l,\phi_l) & \sum_{s=1}^{S}\sum_{q=1}^{Q}[U_{sM}G_{sqM}^1 + V_{sM}G_{sqM}^2 + W_{sM}G_{sqM}^4] & \sum_{s=1}^{S}\sum_{q=1}^{Q}[-V_{sM}G_{sqM}^3 - W_{sM}G_{sqM}^5] \end{bmatrix} \begin{bmatrix} E_l^{(k)} \\ B_{sq}^{(k)} \\ C_{sq}^{(k)} \\ \end{bmatrix} \tag{4.16}$$

Here it is assumed that scatterers are exterior to the array elements and each scatterer is approximated as a sphere whose radius is ρ_s. The number of harmonics required to sufficiently represent the scattered field from a near-zone scatterer can be approximately given as $Q = \beta r_s$. Equal number of harmonics for each scatterer is also assumed for simplicity. Here the unknowns are $E_l^{(k)}$,$B_{sq}^{(k)}$ and $C_{sq}^{(k)}$ where $l = 1,2...,L(k)$,$s = 1,2...,S$ and $q = 1,2...,Q$. Thus, the total number of unknowns in the above equation is given as $N = L^{(k)} + SQ + SQ = L^{(k)} + 2SQ$. As its predecessor [32], we solve Equation (4.16) by the least squares method with the condition that $N < M$.

3. The incident voltage in each iteration is evaluated as

$$V^{inc} = V^t - V^{sct} \tag{4.17}$$

where V^{sct} is found through Equation (4.14) for each antenna by using current values of B and C, the spherical harmonic's amplitudes.

4. The incident voltage from the above step is used to find the elevation of incident sources and the iteration index is incremented and the algorithm is repeated until convergence of the DOA estimate is achieved.

Although there is no surety of achieving the true value or exact DOA, convergence is guaranteed. In the next section, the capability of the method is demonstrated by numerical examples. The Matlab® code for this algorithm is available as Appendix B.

4.3 Results and Discussion

The examples presented in this section test the algorithm for a variety of situations. All examples use horizontal (x-directed) half-wave dipoles of wire radius $\rho_a = 0.001\lambda$ as elements of a uniform linear array. The array principal axis is along the z direction and its first element center is $(0,0,0)$. Examples 1 and 2 have element spacing $d = 0.5\lambda$ and examples 3 and 4 have closely spaced elements with spacing $d = 0.25\lambda$. These examples take into account the more practical radius of antenna element as compared to [32], where it was $\rho_a = 0.00001\lambda$. For example, at $f = 3GHz$, our antenna radius will be $1mm$, where further reduction makes the antenna impractical. The experiment is carried out using the COMSOL® multiphysics environment [43]. The classical method; delay-and-sum [54] is

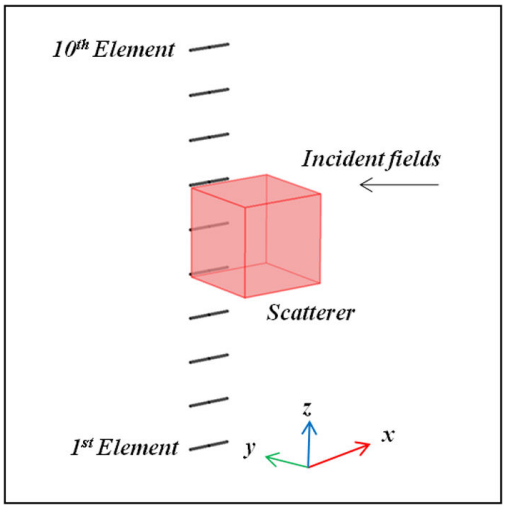

(a) Antenna array and near-zone scatterer for example 1 & 2

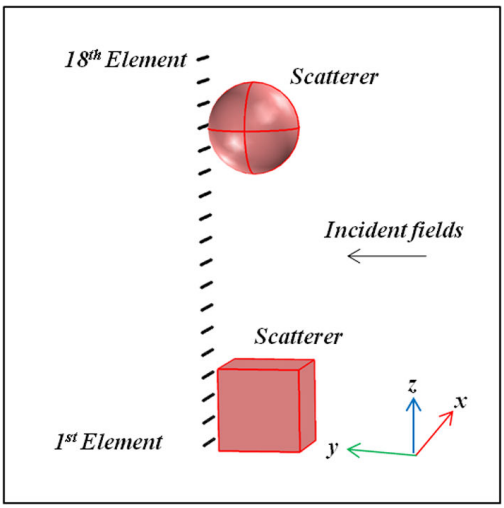

(b) Antenna array and near-zone scatterers for example 3 & 4

Figure 4.3: Geometric setup for examples 1,2,3 & 4

used for DOA estimation. In all of these examples, a source at a particular DOA is detected when the amplitude at that angle equals or exceeds 30% of the maximum amplitude in the spectrum. It is anticipated that $Q = 2$ to 3 harmonics will be sufficient both to represent the field due to the scatterer and for convergence of the solution because all our scatterers have radius $\rho_s \approx 0.5\lambda$ from their geometric center. It should be noted that having Q harmonics in Equation (4.16), will result in $2Q$ unknowns for each scatterer.

Example 1: The setup of this example is shown in Fig. 4.3(a). Here $S = 1$ scatterer , $L = 1$ incident plane wave and $M = 10$ elements. The elevation of the incident wave is $\theta_1 = 60^o$ and the scatterer's (cube of side length$= \lambda$) geometric center is located at $(0.2, -0.6, 2.5)\lambda$. Fig. 4.4(a) shows that the uncorrected DOA spectrum at $k = 0$ detects the incident wave DOA $\theta_1^{(0)} = 59.4^o$ and two spurious DOAs 78^o and 120.3^o. Thus, initially the algorithm has to assume three incident waves. The corrected spectrum shows error reduction for

the desired DOA and suppression of the spurious peaks, to the value below 30% of the maximum value, thereby reducing the number of sources to the correct value of one. The convergence of $\theta_1^{(k)}$ to $\theta_1^{(K)} = 60.3^o$ using $Q = 3$ spherical harmonics is shown in Fig. 4.4(b).

Example 2: This example has the same geometrical setup of example 1, but has two incident plane waves $L = 2$. The elevation of the incident waves is $\theta_1 = 60^o$ and $\theta_2 = 105.0^o$. The algorithm initially estimates two incident waves $\theta_1^{(0)} = 58.8^o$ and $\theta_2^{(0)} = 105.8^o$. Two spurious DOAs 78.8^o and 86.7^o are also detected at $k = 0$ as shown in Fig.4.5. Thus, initially the algorithm has to assume four incident waves. Spurious peaks in the DOA spectrum are successfully reduced and the DOA estimation of desired waves is reasonably achieved. The convergence of $\theta_1^{(k)}$ to $\theta_1^{(K)} = 60.3^o$ and $\theta_2^{(k)}$ to $\theta_2^{(K)} = 105.2^o$ using $Q = 3$ is shown in Fig.4.6.

Example 3: This example is more complex by not only having $S = 2$ scatterers but also having closely spaced antenna elements $d = 0.25\lambda$, which causes an increase in mutual coupling. The geometry is shown in Fig.4.3(b). The number of unknowns will increase as the number of scatterers increases, so in this example more antenna elements $M = 18$ are used to adequately satisfy the least squares optimization condition $N \leq M$. The elevation of the incident wave $L = 1$ is $\theta_1 = 105.0^o$. One scatterer in the form of a cube of side length= 0.9λ is placed at $(-0.2, -0.7, 0.45)\lambda$ and the other as a sphere of radius $\rho_s = 0.5\lambda$ with geometric center at $(-0.2, -0.6, 3.5)\lambda$. Fig.4.7(a) shows the uncorrected DOA spectrum

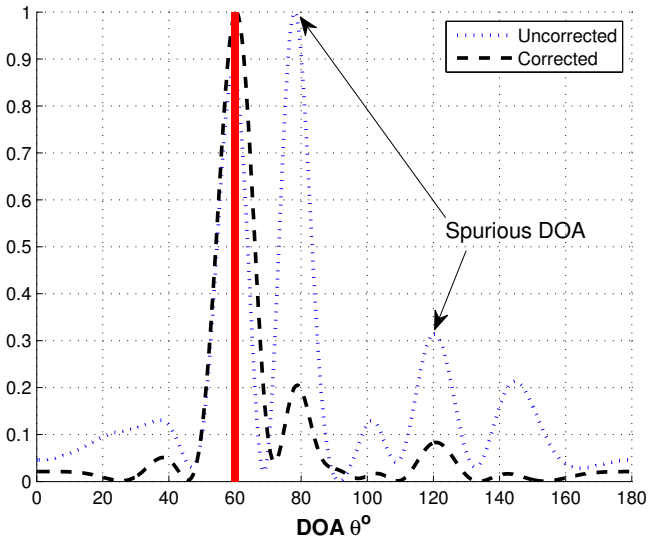

(a) DOA spectrum for example 1

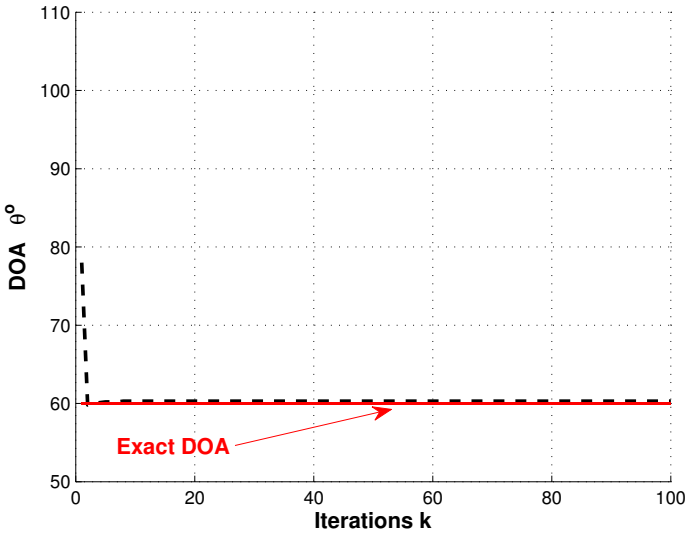

(b) Convergence of $\theta_1^{(k)}$ for example 1

Figure 4.4: Results for example 1

at $k = 0$, where the incident wave DOA is detected as $\theta_1^{(0)} = 103.0^o$ and one spurious DOA at 129.2^o. The corrected spectrum shows improved DOA estimation and snubbing of the spurious peak, thereby reducing the number of sources to the correct value of one.

The convergence of $\theta_1^{(k)}$ to $\theta_1^{(K)} = 104.6^o$ using $Q = 2$ spherical harmonics is shown in Fig.4.7(b).

Example 4: The geometrical setup of this case is the same as for Example 3 , but has two incident plane waves $L = 2$. The elevation of the incident waves is $\theta_1 = 60^o$ and $\theta_2 = 105.0^o$. The algorithm initially estimates three incident waves $\theta_1^{(0)} = 61.0^o$ and $\theta_2^{(0)} = 102.8^o$. One spurious DOA 46.4^o is also detected as shown in Fig.4.8. This case shows the trouble an ordinary DOA estimator (un-calibrated) can face, where the spurious signal peak has almost the same value as of desired signal. Thus, the spurious signal can not be rejected by setting a threshold value as this will also reject the desired signal. Our algorithm takes into account three incident waves initially. After convergence of the algorithm, the unwanted signal peak is almost eradicated and the DOA estimation accuracy is also improved. The convergence of $\theta_1^{(k)}$ to $\theta_1^{(K)} = 59.4^o$ and $\theta_2^{(k)}$ to $\theta_2^{(K)} = 105.4^o$ using

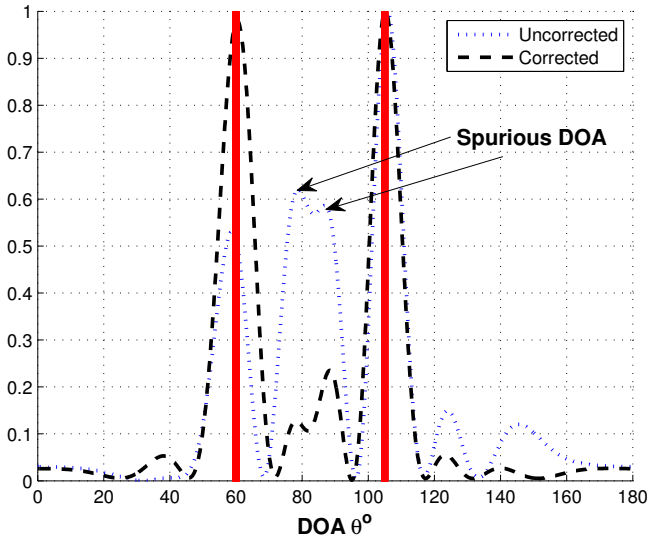

Figure 4.5: DOA spectrum for example 2

$Q = 2$ is shown in Fig.4.9. This example also shows the slower and erratic convergence of the solution due to the complexity of the situation. This iterative nature of the solution is a drawback of this method. From this, it is worth to mention that an approximately similar

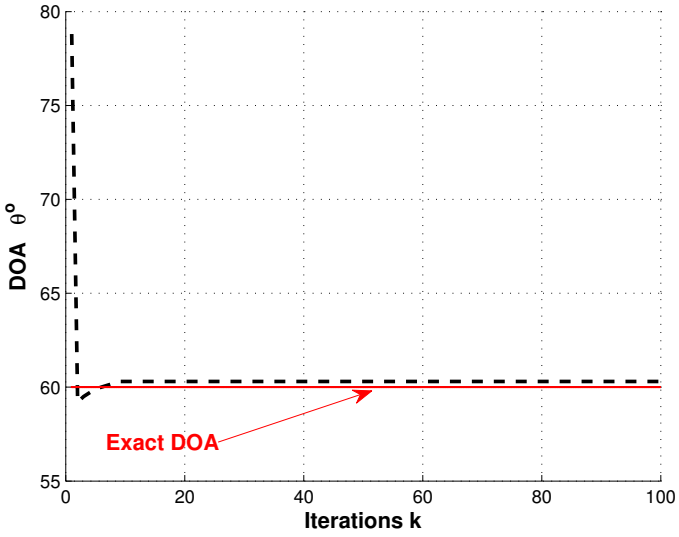

(a) Convergence of $\theta_1^{(k)}$

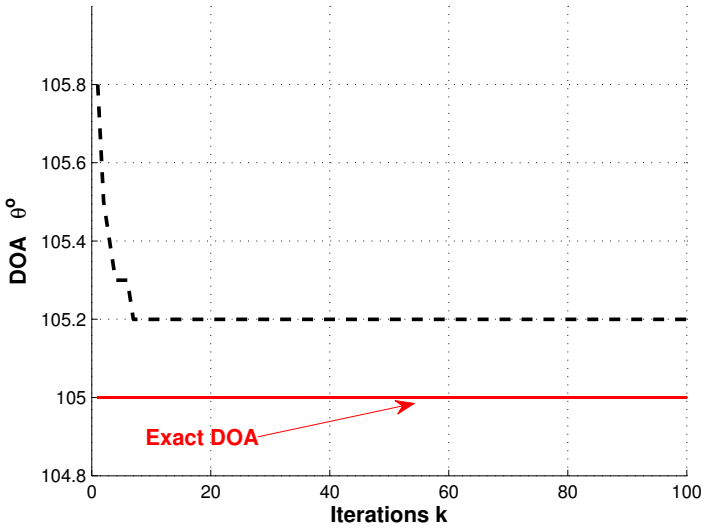

(b) Convergence of $\theta_2^{(k)}$

Figure 4.6: Convergence of $\theta_1^{(k)}$ and $\theta_2^{(k)}$ for example 2

geometric situation was handled by $M = 45$ antenna elements using cylindrical harmonics [32].

A summary of the number of iterations required and the convergence time using Intel®

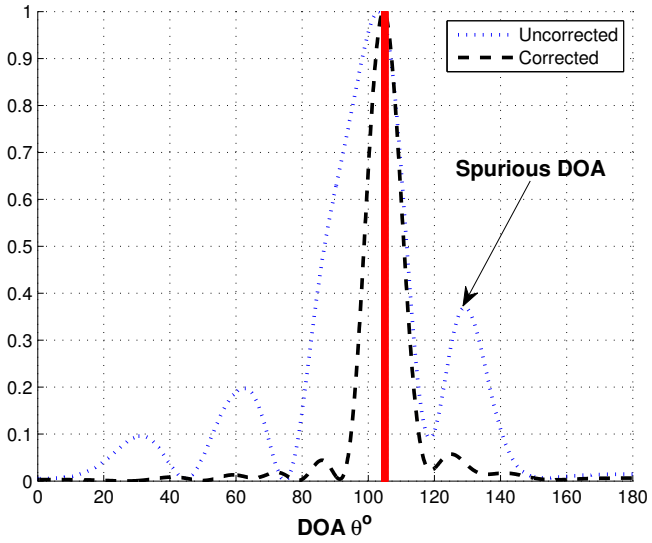

(a) DOA spectrum for example 3

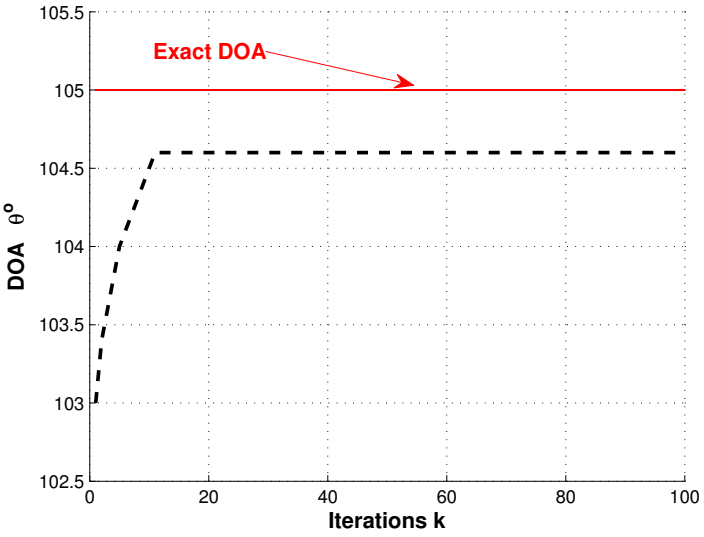

(b) Convergence of $\theta_1^{(k)}$ for example 3

Figure 4.7: Results for example 3

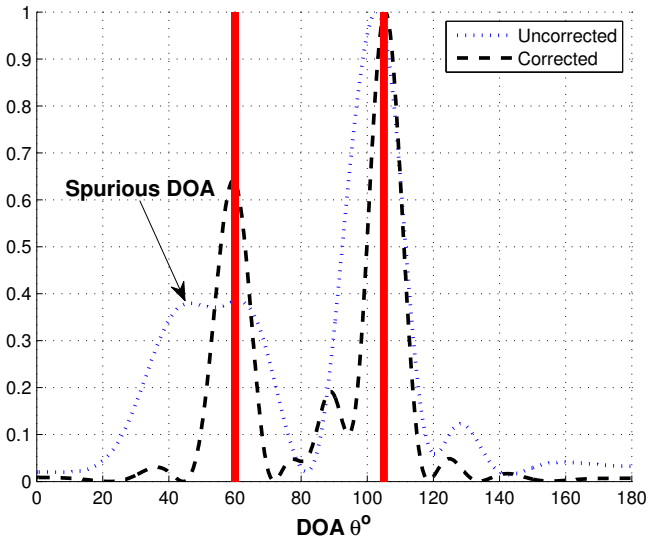

Figure 4.8: DOA spectrum for example 4

core^{TM}i5-2500 processor is given in Table.4.1. The number of iterations and convergence time increase as the complexity increases. However, with faster processing, the processing time can be further reduced. The received terminal voltages in COMSOL ® for Examples 1-4 are available in Appendix C.

Table 4.1
Number of iterations and convergence time for examples 1-4

Examples #	Iterations K #	Convergence time Seconds
1	10	0.33
2	10	0.33
3	12	0.392
4	78	2.23

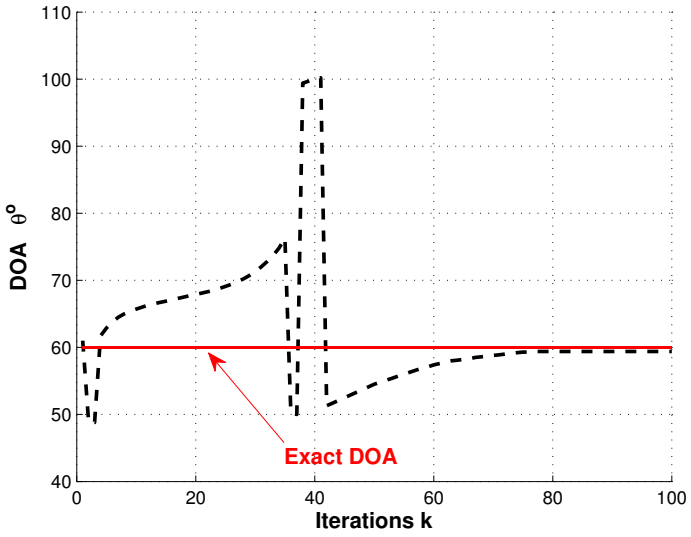

(a) Convergence of $\theta_1^{(k)}$

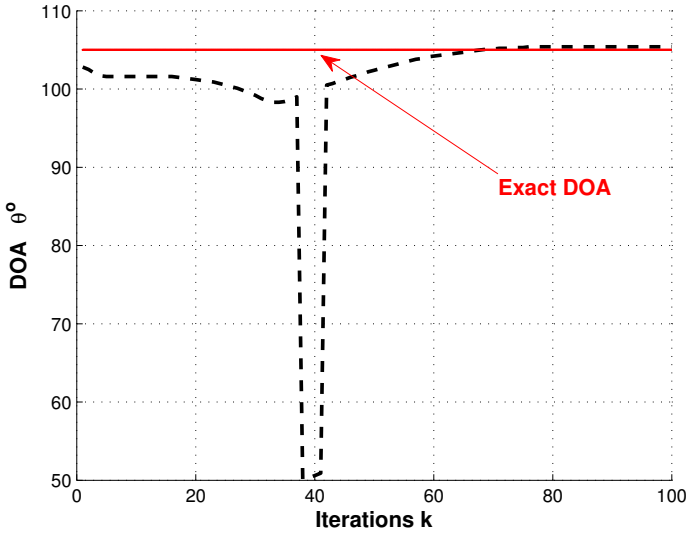

(b) Convergence of $\theta_2^{(k)}$

Figure 4.9: Convergence of $\theta_1^{(k)}$ and $\theta_2^{(k)}$ for example 4

4.4 Conclusion

The auto-calibration method described here extends the state-of-the-art method available in DOA estimation in the presence of near-zone 3D scatterers. The work is supported by numerical examples for a variety of complex situations in terms of multiple incident waves and scatterers. Use of spherical harmonics provides a better realization of the scattering field with a fewer number of harmonics and, therefore, reduces the number of antenna elements required in comparison with using cylindrical harmonics. Although this approach is demonstrated to be more practical in terms of using 3D scatterers and real size antenna elements, it still carries the same two drawbacks: due to the iterative method, it has limited application to cases where time delay is acceptable and, secondly, as the electrical size or number of scatterers increases, the number of unknowns increase, which requires more antenna elements. However, the method motivates the researchers towards a more realistic situation. Finding a guaranteed solution with this method is one of the open problems. Scenarios when multiple scatterers come close to each other and also to antenna elements result in mutual coupling between scatterer-scatterer and scatterer to antenna are yet to be addressed, to the best of our knowledge.

4.5 Nomenclature

B_{sq}, C_{sq}	Spherical harmonic's amplitudes
d	Element spacing in wavelength λ
E_l	Amplitudes of lth incident plane wave
E^t	Total electric field
E^{inc}	Incident electric field
E^{sct}	Scattered electric field from scatterer
f	Frequency of incident signal
$G^1_{sqm}, \ldots, G^5_{sqm}$	Spherical harmonics
$\hat{H}^{(2)}$	Spherical Hankel function of second kind
$\hat{H}^{(2)'}$	First derivative of spherical Hankel function of second kind
$\hat{H}^{(2)''}$	Second derivative of spherical Hankel function of second kind
L	Number of incident plane waves
l	Incident plane wave index
M	Number of antenna elements
m	Antenna element index
N	Number of unknowns in the set of simultaneous linear equations
P^1	Associated Legendre function of first kind
P'^1	First derivative of associated Legendre function of first kind
PW	Plane wave

Q	Number of spherical harmonics used
q	Index of spherical harmonic
r	Radial distance in spherical coordinates
r_{sm}	Radial distance from sth scatterer to mth element
S	Number of Scatterers
s	Scatterer index
U, V, W	Constants for fixed element and scatterer location
(x_m, y_m, z_m)	Location of mth antenna element in cartesian coordinates
(x_s, y_s, z_s)	Location of sth scatterer in cartesian coordinates
β	Free space wave number
θ	Elevation angle in spherical coordinates
θ_{sm}	Elevation angle of mth element from sth scatterer
(θ_l, ϕ_l)	Incidence direction of lth plane wave
ρ_a	Radius of antenna wire
ρ_s	Radius of scatterer
ϕ	Azimuth angle in spherical coordinates
ϕ_{sm}	Azimuth angle of mth element from sth scatterer

Chapter 5

Conclusion

Direction-of-arrival estimation is prone to various errors. One major source of error is the assumption that array elements are independent of one another. In reality, radiation from one element interacts with other elements. This phenomenon is known as mutual coupling. Various techniques are available in the literature to compensate for this error, but generally these methods assume antennas are placed in free-space; thus, effects of the presence of an arbitrary ground are neglected. A second significant source of error is the assumption that the surroundings of the array is free of any other resonating object but, that in general, the DOA estimation is deeply affected by the presence of near-zone objects or scatterers. This work addresses both of the above errors; first, by introducing pre-calibration to remove antenna mutual coupling effects on DOA estimation in the presence of a real-earth and, second, by presenting a self-calibration algorithm to remove the effects of 3D scatterers on

DOA estimation.

Effects of ground parameters on mutual coupling of wire type antenna arrays for DOA estimation are investigated. Both monopole and dipole antenna elements are included in the research and to the best of the authors' knowledge novel results are presented. While monopole antenna arrays need a ground plane for their operation using image theory, dipole arrays show significant variation in the performance for an antenna height $h < 0.25\lambda$ from the ground.

Significant impact of ground constituent parameters on mutual impedance of a monopole array is observed. As a rule of thumb, we suggest reducing the values of mutual impedance between two vertical monopoles be reduced to 50% of the values found in the anechoic chamber over a perfect ground for applications on a real-earth. The increase of RMSE in the case when the antenna is placed over poor ground and pre-estimated mutual impedance matrix (assuming perfect ground) is used to remove errors in DOA, underscores the importance of this investigation. We propose that the technique of estimating mutual coupling presented in [17] is applicable to all ground conditions, provided the antennas be placed on respective grounds.

Investigation of mutual impedance of dipole array showed insensitivity to the variations in the ground conductivity after an antenna height $h \geq \lambda$. Results for both horizontal and vertical polarization depicted a similar trend of insensitivity. This outcome supports the application of an existing technique [17] to the real-earth situations. The invariance

of RMSE of DOA estimation to antenna height measured from a typical good-ground suppresses concerns for using the existing method for removing received mutual coupling effects on DOA estimation near real-ground. Thus, the existing compensatory techniques for removing mutual coupling associated errors from DOA estimation can be safely used for antenna height $h \geq \lambda$. We also propose that the very same techniques can also be marginally used for antenna height $h \geq 0.25\lambda$.

An auto-calibration method is presented that extends the state-of-the-art method available in DOA estimation in the presence of near-zone 3D scatterers. A number of numerical examples for a variety of complex situations, in terms of multiple incident waves and scatterers, are also appended. Spherical harmonics are used to provide better realization of the scattering field from the near-zone scatterer. Results showed that fewer antenna elements are required when using spherical harmonics instead of cylindrical harmonics. Despite the method's practicability in terms of using 3D scatterers and real-size antenna elements, it still has the same two drawbacks: firstly being an iterative method, it has limited application to situations where time delay is acceptable and, secondly, as the electrical size and/or number of scatterers increases, the number of unknowns increases, which requires more antenna elements.

To the best of the author's knowledge this research motivates a number of open problems in this area as the realization of the environment improves. It is understood that it is not always possible to pre-estimate mutual impedance for a variety of ground conditions. It is

also worth noting that most of the DOA estimation techniques in the literature assume the array is in free-space. Therefore, this research also brings to light the need for a universal solution of this issue that can be used for any arbitrary ground condition and polarization. Moreover, suppressing the errors in DOA estimation due to the presence of near-zone scatterers is also an open problem, which has been, until now, addressed with certain constraints. The method developed in this work motivates the contemporary researchers towards a more realistic solution of this problem. Finding a guaranteed solution with this method is also an open problem. A complex, yet-to-be-addressed scenario is possible when multiple scatterers come close to each other and also to the antenna elements, resulting in mutual coupling between scatterer-scatterer and scatterer-antenna. The same problem can suffer an increase of complexity once noise is introduced in the estimation.

In Fig. 5.1 a quagmire is shown, which arises due to the presence of near-zone scatterers and nearness of an arbitrary ground to the DOA estimation array. The solution to this problem may be considered as the first consolidated step in the direction set by this dissertation.

In summary, this work demonstrated the vulnerability of DOA estimation to the presence of a real environment around the antenna array. The knowledge of the surroundings enables the signal processing algorithms to modify themselves for correct DOA estimation. This work investigated the two major sources of error: array mutual coupling in the presence of an arbitrary ground and the presence of 3D scatterers in the near-zone of the antenna array.

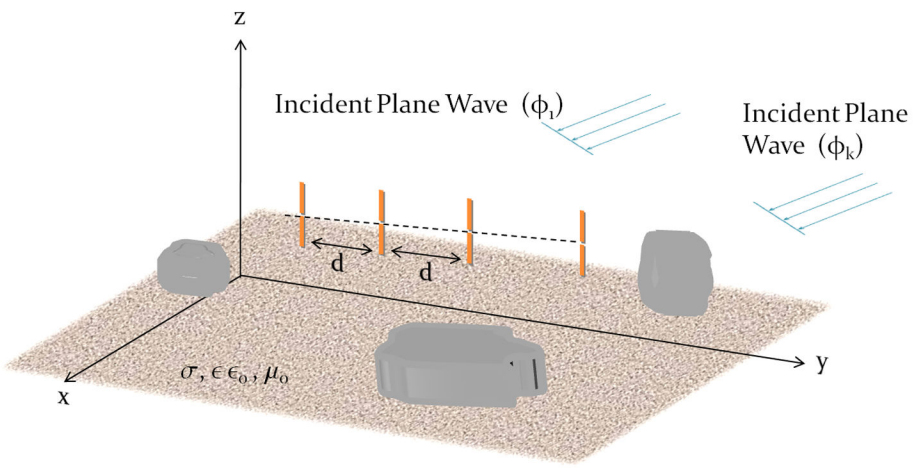

Figure 5.1: Near-ground DOA estimation in the presence of near-zone 3D scatterers

Here, mutual coupling for ULA is preestimated for various ground conditions of array operation using FEM. Secondly, a self-calibration algorithm is presented for suppression of errors due to the presence of 3D scatterers. This work has constraints such as antenna type, array structure, polarization, scatterer shape and knowledge of scatterer location. These limitations invite researchers towards further open problems in this area.

Appendix A

Procedure for Finding Z_{12} in Chapters 2 and 3

The procedure being described here to find mutual impedance between two wire type antennas is an extension of the method found in [17]. Consider $\lambda/4$-monopole antenna elements as shown in Fig. 2.1 for estimating mutual impedance Z_{12} between the elements. The array is operating at a frequency of 2.4 GHz and connected to a terminal load $Z_L = 50\Omega$. The length of the antenna element is l =30 mm, the element radius is ρ_a =0.3 mm and the element spacing is $d = \lambda/2$ which equals 62.5 mm. The array is placed over an arbitrary ground whose constituent parameters $(\sigma, \varepsilon, \mu)$ can be altered to match the specification of a particular ground type as described in Table 2.1. The simulation is carried out in COMSOL® multiphysics environment[43]. The array is in receiving mode and vertically

polarized plane wave incidence is considered from a direction ($\theta = 90^o, \phi$). It is well known that for wire type antennas the mutual impedance estimation is independent of azimuth (ϕ) direction for a given elevation angle (θ). The mutual impedance Z_{12} is dependent on the values of W_1^t and I_2^t as shown in (2.6). The voltage W_1^t can be described as (2.5):

$$W_1^t = V_1^t - U_1^t. \tag{A.1}$$

The voltage U_1^t is measured at the antenna terminal #1 in isolation from the second antenna that is by removing the second antenna element. On the other hand voltage V_1^t is measured at the antenna terminal #1 in the presence of antenna #2. The current I_2^t can be defined as:

$$I_2^t = \frac{V_2^t}{Z_L} \tag{A.2}$$

where V_2^t is measured at antenna terminal #2 in the presence of antenna #1. Thus the mutual impedance equation (2.9) can be represented in terms of measurable parameters as following:

$$Z_{12} = \frac{V_1^t - U_1^t}{V_2^t} Z_L. \tag{A.3}$$

This procedure can be used for estimation of mutual impedance Z_{12} of vertical and

horizontal dipole arrays for geometries shown in Fig.3.1 and Fig.3.4 respectively. Table A.1 is presented to show the voltages at antenna terminals for producing plots in Fig. 2.3.

Table A.1
Terminal voltages in volts from COMSOL for Fig. 2.3

Ground Type	U_1^t	V_1^t	V_2^t
Poor Ground	-8.2075e-7+2.2877e-7i	-8.5272e-7+2.0014e-7i	-8.5121e-7+1.9815e-7i
Typical Ground	-6.7185e-7+1.6515e-7i	-7.1341e-7+1.2074e-7i	-7.1274e-7+1.1904e-7i
Good Ground	-5.9035e-7+1.4024e-7i	-6.3118e-7+9.3633e-8i	-6.3073e-7+9.2087e-8i
Sea Water	-4.0372e-7+9.0667e-8i	-4.366e-7+4.791e-8i	-4.3644e-7+4.6765e-8i
Fresh Water	-4.0627e-7+1.1491e-7i	-4.4607e-7+7.4001e-8i	-4.4601e-7+7.2865e-8i
Copper	-4.8613e-6+1.0729e-6i	-5.3522e-6+3.0549e-7i	-5.3531e-6+2.8972e-7i

Appendix B

Matlab® Code for DOA Estimation Algorithm in Chapter 4

Matlab® is a registered trade mark

```
%*****************************************************************
%  THIS IS A MATLAB  BASED PROGRAM AND IS BASED ON THE ALGORITHM
%   PRESENTED IN CHAPTER 4
%*****************************************************************
%                        Written by:
%      Irfan Ahmed and Dr. Warren F. Perger, 2011
%             Michigan Technological University
%                      Houghton MI, USA
%*****************************************************************
```

```
%                          COMPUTES:
%   I. Antenna Element Positions (assuming ULA along  z axis)%
%  II. Element Position Relative to Scatterer in spherical Coordinates
% III. Associated Legender  function and its derivative
%  IV. Spherical Hankel function and its derivative
%   V. All Harmonics needed for Algorithm G_1 to G_5
%  VI. Direction-of-Arrival (elevation angle) both crude and accurate
%
%                       INPUT PARAMETERS:
%     1. Number of Elements M
%     2. VERTICAL DISPLACEMENT OF DIPOLES d
%     3. Z-coordinate of first antenna element
%     4. Number of Scatterers S
%     5. Cartesian coordinates of each scatterer
%     6. Number of Harmonics to be evaluated Q
%
%**   NOTE: ALL THE INPUT LENGTH PARAMETERS ARE IN WAVELENGTHS.
%*********************************************************
clear all
close all
beta = 2*pi; % Wave number
%c=3e8;%Speed of light in vacuum

% Input Array parameters assuming ULA
prompt={'Enter the number of array elements, M:',...
```

```
        'Enter the element spacing in wavelengths, d:',...
        'Location of the first antenna element, z_1'};
name='Input for Array configuration';
numlines=1;
defaultanswer={'10','0.5','0'};
array_input=inputdlg(prompt,name,numlines,defaultanswer);
array_input=str2double(array_input);

% Input Scatterer quantity
prompt={'Enter the number of scatterers, S:',...
    'Enter the spherical harmonics to be evaluated, Q:'};
name='Input Number of Scatterer elements';
numlines=1;
defaultanswer={'1','3'};
scatterer_input=inputdlg(prompt,name,numlines,defaultanswer);
scatterer_input=str2double(scatterer_input);
% Input Scatterer Location
S=scatterer_input(1);
if S>0
 for s = 1:S
     prompt={'Enter the x, x_s:' ,'Enter the y, y_s:',...
         'Enter the z, z_s:'};
name='Input Number of Scatterer elements ';
numlines=1;
defaultanswer={'0.2','-0.6','2.5'};
```

```
sc(:,s)=inputdlg(prompt,name,numlines,defaultanswer);
s_coord=str2double(sc(:,:)');
  end
%************************************************
% Evaluate Array coordinates along z axis
M=array_input(1);
d=array_input(2);
z_1_array=array_input(3);
z_m_coord=z_1_array+d*(0:M-1);
m_coord=[(0*(1:M))' (0*(1:M))' (z_m_coord)'];
%[x1 y1 z1;...;xm ym zm]

%Evaluate Scatterer Location w.r.t antenna elements in spherical
%coordinates
for s=1:S
    for m=1:M
     x_sm(m,1,s)=[m_coord(m,1)-s_coord(s,1)];
     y_sm(m,1,s)=[m_coord(m,2)-s_coord(s,2)];
     z_sm(m,1,s)=[m_coord(m,3)-s_coord(s,3)];
     r_sm_vec(m ,[1:3],s)=[ (x_sm(m,1,s))...
          (y_sm(m,1,s)) (z_sm(m,1,s)) ];
     r_sm(m,1,s)=sqrt((x_sm(m,1,s))^2+(y_sm(m,1,s))^2+...
          (z_sm(m,1,s))^2);
     theta_sm(m,1,s)=acos(dot(r_sm_vec(m,:,s),[0 0 1])...
          /r_sm(m,1,s));
```

```
      phi_sm(m,1,s)=acos(dot(r_sm_vec(m,:,s),...
          [1 0 0])/(r_sm(m,1,s)*sin(theta_sm(m,1,s))));
    end
end
sm_coord=[r_sm theta_sm phi_sm];
% ...[r1 theta1 phi1;....;rsm theta_sm phi,sm]
else
  error('S=0, This program works for S>1')
end
% Evaluation of Constants Usm Vsm and Wsm
U_sm=-1i*sin (sm_coord(:,2,:)).*...
    (cos(sm_coord(:,3,:))).^2;%[u11; u12;...usm]
V_sm= (cos((sm_coord(:,2,:)).*(cos(sm_coord(:,3,:))).^2))...
    ./(beta*(sm_coord(:,1,:)));%[v11; v12;...vsm]
W_sm=- (sin(sm_coord(:,3,:))).^2./...
    (beta*(sm_coord(:,1,:)));%[w11; w12;...wsm]
% Evaluation of Spherical Harmonics See Balanis IV-49
Q=scatterer_input(2);
% Separate loop for Legendre poly Q+1 harmonics
P1_a=zeros(M, Q+1,S);
for q=1:Q+1

    P=legendre(q,cos(sm_coord(:,2,[1:S])));
     P2=P(2,:,1,[1:S]);
     % .Select second row of P because...
```

```
    %  ..we want order 1 harmonic only
    P3=permute(P2,[2 1 3 4]);
     P1_a(:,q,[1:S])=P3; % MxQxS ;P^1
end
P1=P1_a(:,[1:Q],:);% P_n^1 harmonics of Legender M x Q x S
%Derivative  P_n^'1 w.r.t cos(theta_sm) M x Q x S
for  q=1:Q
P1_d(:,q,[1:S])=(-1-q)*...
    cos(sm_coord(:,2,[1:S])).*P1_a(:,q,[1:S])...
    +q.*P1_a(:,q+1,[1:S])./(-1+(cos(sm_coord(:,2,[1:S]))).^2);
end
% Hankel functions  Mx Qx S
for q=1:Q
H_2(:,q,[1:S])=sqrt(pi*2*pi*sm_coord(:,1,[1:S])/2).*...
    (besselh(q+0.5,2,2*pi*sm_coord(:,1,[1:S])));
end
%First derivative of Hankel function  M x Q x S
for q=1:Q
  H_2_1d(:,q,[1:S])=sqrt(pi/2).*(besselh(q+0.5,2,2*pi*...
      sm_coord(:,1,[1:S]))).*...
      (2*sqrt(2*pi*sm_coord(:,1,[1:S])))...
      +0.5* sqrt(pi*2*pi*sm_coord(:,1,[1:S])/2).*...
      ((besselh(-0.5+q,2,2*pi*sm_coord(:,1,[1:S]))...
      - besselh(q+1.5,2,2*pi*sm_coord(:,1,[1:S]))));
  end
```

```
%Second Derivative of Hankel  M x Q x S
 for q=1:Q
   H_2_2d(:,q,[1:S])=-sqrt(pi/2).*...
        (besselh(q+0.5,2,2*pi*...
        sm_coord(:,1,[1:S]))).*...
        (4*((2*pi*sm_coord(:,1,[1:S]))).^1.5)+...
        sqrt(pi/2)* (besselh(-0.5+q,2,...
        2*pi*sm_coord(:,1,[1:S]))...
        - besselh(q+1.5,2,2*pi*sm_coord(:,1,[1:S]))).*...
        (2*sqrt(2*pi*sm_coord(:,1,[1:S])))+...
        0.5* sqrt(pi*2*pi*sm_coord(:,1,[1:S])/2).*...
        (0.5*(besselh(-1.5+q,2,2*pi*sm_coord(:,1,[1:S]))...
        - besselh(q+0.5,2,2*pi*sm_coord(:,1,[1:S])))+...
        0.5*(-(besselh(0.5+q,2,2*pi*sm_coord(:,1,[1:S]))...
        + besselh(q+2.5,2,2*pi*sm_coord(:,1,[1:S]))));
 end
%Spherical Harmonics G^1 to G^5 order M x Q x S
G_1=(H_2_2d+H_2).*P1; %
for q=1:Q
   G_2_a(:,q,[1:S])= sin(sm_coord(:,2,[1:S])).*...
        P1_d(:,q,[1:S]);end
 G_2=1i*H_2_1d.*G_2_a;
for q=1:Q
   G_3_a(:,q,[1:S])= P1(:,q,[1:S]).*...
        sin(sm_coord(:,2,[1:S]));
```

```
end
G_3=-H_2.*G_3_a;
% Multiply by minus sign'- 'to make final equation form positive
G_4=1i*H_2_1d.*G_3_a;
G_5=-H_2.*G_2_a;
% Multiply by minus sign '-'to make final equation form positive
%  Multiply U, V, W with  corresponding G's
for q=1:Q
    G_1_u(:,q,[1:S])=U_sm .* G_1(:,q,[1:S]);
    G_2_v(:,q,[1:S])=V_sm .* G_2(:,q,[1:S]);
    G_3_v(:,q,[1:S])=V_sm .* G_3(:,q,[1:S]);
    G_4_w(:,q,[1:S])=W_sm .* G_4(:,q,[1:S]);
    G_5_w(:,q,[1:S])=W_sm .* G_5(:,q,[1:S]);
end
%Rearranging Gs according to unknowns  B and C
G_B1=G_1_u+G_2_v+G_4_w;
G_C1=G_3_v+G_5_w;
G_B=reshape(G_B1,M,Q*S); % order M x Q*S
G_C=reshape(G_C1,M,Q*S);% order M x Q*S
%************************************************
% Load V^t from COMSOL Data stored in Excel file
Nsam=1;% Number of samples from COMSOL
[a v]=xlsread('\Example-1\horz-dip10_s1_J1');
v_t_s=str2double(v(:,1));
tic % begn time check
```

```
x =v_t_s ;% Actual Received Signal
if (length(v_t_s)==M)
% Calculating The covariance matrix of the received signal
R=x*x'/Nsam;
%%%%% Computing Classic Spectrum---- Dealy-and-sum%%%%
%%%%DOA Estimation before correction
angles=(0:0.1:180)*pi/180;
%.. Range of angles for which DOA sorted.
v_ideal= exp(-1i*2*pi*(z_1_array+d*(0:M-1))'...
    *cos(angles(:).'));
for i= 1:length(angles)
       classic1(i)=v_ideal(:,i)'*R*v_ideal(:,i);
end
[pks1,locs] = findpeaks(abs(classic1),'sortstr','descend');
p_2=pks1(pks1>=0.3*pks1(1)); %30% above highest peak is a source
L=length(p_2); %Estimated Number of sources before correction
else
  error( 'M is not equal to the number of  terminal voltages')
end


%************************************************
% Iterative Algorithm
k=1;
% e=1;
%while e>0.00001 Our Examples converged within ...
```

```
%100 iteration otherwise a while loop can be used
for k=1:100
p(k,:)=angles(locs(1:L));
p1(k,:)=p(k,:)*180/pi
v_pw= exp(-1i*2*pi*(z_1_array+d*(0:M-1))'...
    *cos(p(k,:))); % M x L
coeff=horzcat(v_pw,G_B,G_C);  % order M x (L+ 2*QS)
% Solve Least square
unknown=coeff\v_t_s;
A(:,k)=unknown(1:L); % Source amplitudes
B(:,k)=unknown(L+1:L+Q*S);% Harmonic amplitudes
C(:,k)=unknown(L+1+Q*S:L+2*Q*S);%Harmonic amplitudes
v_i(:,k)=v_t_s-G_B*B(:,k)-G_C*C(:,k);
% Find DOA
R=v_i(:,k)*v_i(:,k)'/Nsam;
for i= 1:length(angles)
        classic(i)=v_ideal(:,i)'*R*v_ideal(:,i);
end
[pks,locs] = findpeaks(abs(classic),'sortstr','descend');
% p1_new(k,:)=angles(locs(1:L))*180/pi;
% e=abs(p1(k,:)-p1_new(k,:))
% k=k+1;
end
toc %end time check
%************************************************
```

```
%Number of sources after correction
p_3=pks(pks>=0.3*pks(1)); %30% above the highest peak is a source
L_new=length(p_3); %Estimated Number of sources after correction
%Plots of Convergence and DOA Estimation ;
grid on
hold on
%Plot of convergence
for i=1
plot(1:length(p1),p1(:,i),'--k','LineWidth',2 )
end
plot(1:0.01:k,60,'-r','LineWidth',1 )
% The value 60 is for known incidence and replaceable
ylabel('DOA   \theta^o',...
    'fontsize',12,'fontweight','b')
xlabel('Iterations k',...
    'fontsize',12,'fontweight','b')
hold off
%Plot of DOA Spectrum Delay-and-Sum
figure
hold on
grid on
ang=angles*180/pi;
plot(ang,(abs(classic1))/pks1(1),...
    ':b','LineWidth',2,'MarkerSize',2)
plot(ang,(abs(classic))/pks(1),...
```

```
    '--K','LineWidth',2,'MarkerSize',6)
xlabel('DOA \theta^o',...
    'fontsize',12,'fontweight','b');
legend('Uncorrected',...
    'Corrected','fontsize',12,'fontweight','b');
plot(60, 0:0.001:1,...
     '-r','LineWidth',4,'MarkerSize',6);
plot(105, 0:0.001:1,...
     '-r','LineWidth',4,'MarkerSize',6);
```

Appendix C

Received Voltages in COMSOL for Examples 1-4 of Chapter 4

Table C.1
Received voltages in volts from COMSOL for Examples 1-2

Antenna Terminal #	Example #1	Example #2
1	-0.0017+0.0015i	-0.0083+0.0065i
2	0.0034+0.0032i	-0.003-3.8182e-4i
3	0.0024-6.6262e-4i	0.0028-0.008i
4	-0.0012-0.011i	-2.7944e-4-0.0136i
5	1.5949e-4-0.0012i	9.2781e-5-0.0017i
6	5.6958e-4-7.0853e-4i	-2.4011e-4-0.001i
7	-0.0021-9.2185e-4i	-0.0022-8.3313e-4i
8	-0.0036-0.0012i	-0.0119+0.0044i
9	-0.0025+0.0025i	-0.0109+0.0034i
10	0.002+0.0062i	-0.0013+9.9695e-4i

Table C.2
Received voltages in volts from COMSOL for Examples 3-4

Antenna Terminal #	Example #3	Example #4
1	4.589e-4+0.0015i	4.5873e-4+0.0016i
2	7.9072e-4+4.3038e-4i	0.0013+4.4112e-4i
3	-2.32e-4+3.7551e-4i	7.8144e-5+3.5628e-4i
4	-0.0011+2.8473e-4i	-9.9047e-4-2.989e-6i
5	8.0612e-5-7.4954e-4i	4.6546e-4-0.0017i
6	0.0031-0.0021i	0.0035-0.0039i
7	0.0057-0.0026i	0.0045-0.0052i
8	0.0063-0.0016i	0.0031-0.0041i
9	0.0045+3.477e-4i	9.5777e-4-2.3394e-4i
10	0.0024+0.002i	7.2674e-4+0.0054i
11	0.0017+0.0028i	0.0028+0.0095i
12	0.0018+0.0024i	0.0047+0.0082i
13	0.002+0.0018i	0.0042+0.0027i
14	0.0024+0.0027i	0.0017+6.5016e-4i
15	0.0017+0.0032i	-0.0013+0.0037i
16	3.3427e-5+8.6385e-4i	-0.0019+0.0041i
17	-9.3702e-4-9.5583e-4i	-0.0012+0.0017i
18	-0.0022-0.0027i	-0.0024-0.0017i

References

[1] K. W. Kolodziej and J. Hjelm, *Local Positioning Systems: LBS Applications and Services*. CRC Press, 2006.

[2] E. Tuncer and B. Friedlander, Eds., *Classical and Modern Direction-of-Arrival Estimation*. Academic Pr, 2009.

[3] H. L. V. Trees, *Optimum Array Processing*. John Wiley and Sons, 2002, vol. IV.

[4] C. Balanis, *Antenna Theory: Analysis and Design*, 2nd ed. New York: Wiley, 1997.

[5] J. D. Kraus, *Antennas: for All Application.*, 3rd ed. Mc Graw Hill, 2002.

[6] M.Wax, S. Tie-Jun, and T. Kailath, "Spatio-temporal spectral analysis by eigenstructure methods," *IEEE Transactions on Acoustics, Speech and Signal Processing*, vol. 32, no. 4, pp. 817 – 827, 1984.

[7] S. Chandran, Ed., *Advances in Direction-of-Arrival Estimation*. Artech House, INC., 2006.

[8] H. Krim and M. Viberg, "Two decades of array signal processing research: the parametric approach," *IEEE Signal Processing Magazine*, vol. 13, no. 4, pp. 67 –94, Jul. 1996.

[9] R. Schmidt, "Multiple emitter location and signal parameter estimation," *IEEE Transactions on Antennas and Propagation*, vol. 34, no. 3, pp. 276–280, 1986.

[10] R. Roy and T. Kailath, "ESPRIT-estimation of signal parameters via rotational invariance techniques," *IEEE Transactions on Acoustics, Speech and Signal Processing*, vol. 37, no. 7, pp. 984 –995, 1989.

[11] J. C. Liberti and T. S.Rappaport, *Smart Antennas for Wireless Communications: IS-95 and Third Generation CDMA Applications*. Prentice Hall PTR, 1999, 553614.

[12] L. C. Godara, *Smart Antennas*. CRC press, 2004.

[13] A. Barabell, "Improving the resolution performance of eigenstructure-based direction-finding algorithms," in *IEEE International Conference on Acoustics, Speech, and Signal Processing ICASSP 83*, vol. 8, 1983, pp. 336–339.

[14] B. Friedlander, "The Root-MUSIC algorithm for direction finding with interpolated arrays," *Signal Process.*, vol. 30, pp. 15–29, January 1993.

[15] I. Gupta and A. Ksienski, "Effect of mutual coupling on the performance of adaptive arrays," *IEEE Transactions on Antennas and Propagation*, vol. 31, no. 5, pp. 785–791, 1983.

[16] J. L. Allen and B. L. Diamond, "Mutual coupling in array antennas," MIT Lincoln Lab., Tech. Rep. 424, 1966.

[17] H. T. Hui, "A new definition of mutual impedance for application in dipole receiving antenna arrays," *IEEE Antennas and Wireless Propagation Letters*, vol. 3, pp. 364–367, 2004.

[18] B. Friedlander and A. J. Weiss, "Direction finding in the presence of mutual coupling," *IEEE Transactions on Antennas and Propagation*, vol. 39, no. 3, pp. 273–284, 1991.

[19] Wikipedia, "Band matrix — wikipedia, the free encyclopedia," 2011, [Online; accessed 21-November-2011]. [Online]. Available: http://en.wikipedia.org/w/index.php?title=Band_matrix&oldid=443759804

[20] M. K. Ozdemir, H. Arslan, and E. Arvas, "Mutual coupling effect in multiantenna wireless communication systems," in *Global Telecommunications Conference, 2003. GLOBECOM '03. IEEE*, vol. 2, 2003, pp. 829–833.

[21] K. Kim and T. K. Sarkar, "Direction-of-arrival (DOA) estimation using a single snapshot of voltages induced in a real array operating in any environment," *Microwave and Optical Technology Letters*, vol. 32, no. 5, pp. 335–340, 2002.

[22] S. Burintramart, T. K. Sarkar, Y. Zhang, and M. Salazar-Palma, "Nonconventional least squares optimization for DOA estimation," *IEEE Transactions on Antennas and Propagation*, vol. 55, no. 3, pp. 707–714, 2007.

[23] E. M. Friel and K. M. Pasala, "Direction finding with compensation for a near field scatterer," in *Antennas and Propagation Society International Symposium, 1995. AP-S. Digest*, vol. 1, 1995, pp. 106–109.

[24] S. Fabrizio and S. Alberto, "A novel online mutual coupling compensation algorithm for uniform and linear arrays," *IEEE Transactions on Signal Processing*, vol. 55, no. 2, pp. 560–573, 2007.

[25] Y. Zhongfu, D. Jisheng, X. Xu, and W. Xiaopei, "DOA estimation for uniform linear array with mutual coupling," *IEEE Transactions on Aerospace and Electronic Systems*, vol. 45, no. 1, pp. 280–288, 2009.

[26] T. Su, K. Dandekar, and H. Ling, "Simulation of mutual coupling effect in circular arrays for direction-finding applications," *Microwave and Optical Technology Letters*, vol. 26, no. 5, pp. 331–336, 2000.

[27] K. R. Dandekar, L. Hao, and X. Guanghan, "Experimental study of mutual coupling compensation in smart antenna applications," *IEEE Transactions on Wireless Communications*, vol. 1, no. 3, pp. 480–487, 2002.

[28] Y. Bin, Y. Chengyou, and H. Ye, "Calibration method for mutual coupling between elements based on parallel genetic algorithm," *The Sixth World Congress on Intelligent Control and Automation, 2006. WCICA 2006.*, vol. 1, pp. 3490–3493, 2006.

[29] H. Gao, X. Zheng, and J. Li, "Estimation of mutual coupling coefficient by simulated annealing algorithm," in *6th International SYmposium on Antennas, Propagation and EM Theory*, 2003, pp. 275–278.

[30] Q. Li, L. Gan, and Z. Ye, "An overview of self-calibration in sensor array processing," in *6th International SYmposium on Antennas, Propagation and EM Theory*, 2003, pp. 279–282.

[31] S. Henault and Y. M. M. Antar, "Accurate evaluation of mutual coupling for array calibration," in *Computational Electromagnetics International Workshop, CEM*, 2009, pp. 34–37.

[32] Y. Horiki and E. Newman, "A self-calibration technique for a DOA array with near-zone scatterers," *IEEE Transactions on Antennas and Propagation*, vol. 54, no. 4, pp. 1162 – 1166, 2006.

[33] R. Harrington, *Time-Harmonic Electromagnetic Fields*. McGraw-Hill, 1961.

[34] I. Ahmed, W. F. Perger, and S. A. Zekavat, "Effects of ground constituent parameters on array mutual coupling for DOA estimation," *International Journal of Antennas and Propagation*, vol. 2011, 2011.

[35] H. Steyskal and J. S. Herd, "Mutual coupling compensation in small array antennas," *IEEE Transactions on Antennas and Propagation*, vol. 38, no. 12, pp. 1971–1975, 1990.

[36] A. Mirkamali, J. Nateghi, and H. Hadidian, "Evaluation of array calibration methods for DOA estimation in presence of ground mutual coupling and near zone objects," in *Proceedings of the Fourth European Conference on Antennas and Propagation (EuCAP)*, 2010, pp. 1–4.

[37] J. R. Wait, *Antenna Theory Part II*, ser. Inter-university electronics series, R. E.Collin and F. J. Zucker, Eds. New York: McGraw-Hill, 1969, vol. 7.

[38] E. K. Miller, A. J. Poggigo, J. Burke, and E. S. Seld, "Analysis of wire antennas in the presence of a conducting half-space. part I. the vertical antenna in free space," *Canadian Journal of Physics*, vol. 50, no. 9, pp. 879–888, 1972.

[39] T. Sarkar, "Analysis of arbitrarily oriented thin wire antenna arrays over imperfect ground planes." *AEÜ Special reprint from ARCHIV FÜR ELEKTRONIK UND ÜBERTRAGUNGSTECHNIK ELECTRONICS AND COMMUNICATION Band 31*, pp. 449–457, 1977.

[40] T. Rappaport, *Wireless Communications: Principles and Practice*, 2nd ed., ser. Prentice Hall communications engineering and emerging technologies series. New Jersey: Prentice Hall PTR, 2002.

[41] J.D.Jackson, *Classical Electrodynamics*, 3rd ed. New York: Wiley, 1999.

[42] T. T. Zhang, H. T. Hui, and Y. Lu, "Compensation for the mutual coupling effect in the ESPRIT direction finding algorithm by using a more effective method," *IEEE Transactions on Antennas and Propagation*, vol. 53, no. 4, pp. 1552 – 1555, April 2005.

[43] "COMSOL multiphysics modelling and engineering simulation software," 2011. [Online]. Available: http://www.comsol.com/products/rf/

[44] H. T. Hui, "A practical approach to compensate for the mutual coupling effect in an adaptive dipole array," *IEEE Transactions on Antennas and Propagation*, vol. 52, no. 5, pp. 1262–1269, 2004.

[45] M. Hata and T. Nagatsu, "Mobile location using signal strength measurements in a cellular system," *IEEE Transactions on Vehicular Technology*, vol. 29, no. 2, pp. 245 – 252, 1980.

[46] G. Turin, W. Jewell, and T. Johnston, "Simulation of urban vehicle-monitoring systems," *IEEE Transactions on Vehicular Technology*, vol. 21, no. 1, pp. 9 – 16, 1972.

[47] Y. Chan, R. Hattin, and J. Plant, "The least squares estimation of time delay and its use in signal detection," *IEEE Transactions on Acoustics, Speech and Signal Processing*, vol. 26, no. 3, pp. 217 – 222, 1978.

[48] K. L. Kaiser, *Electromagnetic Compatibility Handbook*. CRC Press, 2004.

[49] K. P. Spies and J. R. Wait, "Determining electrical ground constants from the mutual impedance of small coplanar loops," *IEEE Transactions on Antennas and Propagation*, vol. 20, no. 4, pp. 501 – 502, 1972.

[50] H. Hui, "Improved compensation for the mutual coupling effect in a dipole array for direction finding," *IEEE Transactions on Antennas and Propagation*, vol. 51, no. 9, pp. 2498 – 2503, 2003.

[51] A. Sommerfeld, *Partial Differential Equations in Physics*. Academic Press, 1964.

[52] E. K. Miller, A. J. Poggio, G. J. Burke, and E. S. Selden, "Analysis of wire antennas in the presence of a conducting half-space. part ii. the horizontal antenna in free space," *Canadian Journal of Physics*, vol. 50, no. 21, pp. 2614–2627, 1972.

[53] "Elsevier B.V." 2011. [Online]. Available: http://www.elsevier.com/wps/find/authorsview.authors/rights?tab=3#DutiesofAuthors

[54] J. Foutz, A. Spanias, and M. K. Banavar, *Narrowband Direction of Arrival Estimation for Antenna Arrays*. Morgan & Claypool Publishers, 2008.

[55] C. A. Balanis, *Advanced Engineering Electromagnetics*. Wiley, 1989.